Hepatic Myofibroblasts

Hepatic myofibroblasts, characterized by expression of α-SMA and production of ECM, are mainly found in chronically injured livers, irrespective of the etiology, and are morphologically defined as large and spindle-shaped cells with cytoplasmic stress fibers running parallel to the long axis. Myofibroblasts are characterized by several common features based on their ultrastructural analysis, including a prominent rough endoplasmic reticulum, a Golgi apparatus producing collagen, peripheral myofilaments, well-developed cell-to-stroma attachment sites (fibronexus), and gap junctions [17, 18]. The process of myofibroblast differentiation leads to a highly proliferative, migratory, and contractile phenotype. The persisting inflammation is believed to drive and sustain fibrogenesis. Myofibroblasts can release a number of pro-inflammatory molecules and directly contribute to this continuous inflammation [10, 19, 20]. In both experimental and clinical liver fibrosis, there is a close correlation between the regression of liver fibrosis and the disappearance of myofibroblasts. Previous studies have demonstrated that some myofibroblasts undergo cell death by apoptosis, while other myofibroblasts are restored to their quiescent-like state [21•, 22]. This phenomenon has been identified recently, but has a great potential for anti-fibrotic therapy. However, the mechanism underlying "inactivation" of HSC/myofibroblasts in response to toxic liver injury remains unknown. Future investigations are required to determine why a half of HSC/myofibroblasts apoptose during regression of liver fibrosis, while the other half of myofibroblasts survives and undergoes inactivation. Identification of the mechanism of HSC/myofibroblast inactivation, may provide new targets for anti-fibrotic therapy.

Two Experimental Models for the Study of Hepatic Fibrosis

Mouse models have been used for several decades to study fibrogenesis. The two most common methods for modeling experimental liver fibrosis in mice are the administration of carbon tetrachloride (CCl_4) and bile duct ligation (BDL). Each model displays specific characteristics in the evolution of fibrosis.

Administration of CCl_4 leads to centrilobular necrosis, and eventually leads to liver fibrosis and cirrhosis. CCl_4 causes damage of hepatocytes, in which highly reactive free radical metabolites are formed by the mixed function oxidase system, including a CYP2E1-mediated reaction [23]. HSCs are activated following CCl_4 challenges. In this model, fibrosis first develops in pericentral areas and secondarily between central and portal areas, which is called "bridging fibrosis."

The hepatic injury induced by BDL in mice is similar to the condition of human secondary biliary cirrhosis; it is characterized by cholestasis, hepatic inflammation, neutrophil infiltration in the portal tracts, proliferation of cholangiocytes, and portal tract fibrosis. In BDL mice, serum bile acid levels increase by dozens of fold. Bile acids are pro-oxidants directly causing tissue damage mediated by reactive oxygen species (ROS), or indirectly through activation of Kupffer cells to release ROS [24]. The overspill of bile acid stimulates the proliferation of cholangiocytes, resulting in a ductular reaction accompanied by portal inflammation and fibrosis [25•]. Previous studies have showed the importance of portal fibroblasts as contributors to fibrosis in the BDL model [26].

Hepatic Stellate Cells (HSCs)

HSCs are intralobular connective tissue cells representing less than ten percent of the total number of liver cells. Under physiological conditions, HSCs reside in the space of Disse and serve as a major storage of Vitamin A in the mammalian body. HSCs also participate in the homeostasis of the intrahepatic ECM protein turnover by secreting the sufficient amount of ECM molecules required for tissue repair and by releasing MMP and their inhibitors. By virtue of the contractility of their long cytoplasmic processes encircling the sinusoid, HSCs presumably contribute to the regulation of hepatic microcirculation through the sinusoidal capillaries [27].

The liver is the main storage organ for dietary Vitamin A. Vitamin A includes numerous retinoid forms such as retinyl esters, retinol, retinal, retinoic acid, and several provitamin A carotenoids. Retinoids are transported in the form of retinyl esters. Dietary retinoids are absorbed in the small intestine, where they are packaged into chylomicrons for transportation to the lymphatic circulation system. The retinoid-containing chylomicrons are taken up by hepatocytes, wherein retinoids are hydrolyzed to retinol, and bound retinol-binding protein (RBP), to transfer to the HSCs for storage. HSCs are the central cellular site for retinoid storage in healthy animals, accounting for as much as 50–60 % of the total retinoid present in the entire body. Retinoids are stored in the form of retinyl esters in the lipid droplets, which are characteristic of HSCs [28]. In response to liver injury, quiescent HSCs activate and release some of the Vitamin A droplets. Upon activation, HSCs change their morphology, migrate to the site of injury, and upregulate mesenchymal markers such as α-SMA, collagen α1(I), and fibronectin. HSCs differentiate into myofibroblasts in the injured liver and produce ECM [29].

Portal fibroblasts

Portal fibroblasts are resident fibroblasts with a spindle shape which are present in very small numbers in the mesenchyme surrounding the bile ducts. Under normal conditions, they participate in physiological ECM turnover. Portal fibroblasts almost certainly give rise to myofibroblasts during the development of cholestatic liver injury (but not toxic liver injury, [30]). In response to hepatic injury induced by BDL in mice, portal fibroblasts proliferate and are activate to produce ECM at the periphery of the bile ducts [31]. Portal fibroblasts can be distinguished from HSCs due to the lack of oil droplets, including Vitamin A. In addition, they express elastin and Thy-1; elastin, fibulin 2, gremlin 1, and mesothelin (a novel marker) have also been identified as markers of portal fibroblasts [32, 33]. However, during the development of hepatic injury, HSCs slightly express elastin [34]. Thy1 is a T cell marker, which is particularly abundant on the surface of thymocytes and peripheral T cells. Therefore, the question is, what are the specific markers for portal fibroblasts, and how portal fibroblasts can be distinguished from other myofibroblasts in fibrotic liver. In chronic cholestatic disorders, the fibrotic tissue is initially located around portal tracts. Histological findings from fibrotic livers suggested that portal fibroblasts contribute to the overall fibroblasts observed in cholestatic liver injury. However, their role in liver fibrosis is still unclear because of the lack of markers that can definitively determine the presence of portal fibroblasts from the pool of hepatic myofibroblasts. This problem is further complicated by a recent report by Asahina et al., suggesting that portal fibroblats and HSCs may originate from a common progenitor during the embryonic development [7].

Strategies to Detect Hepatic Myofibroblasts

In recent years, manipulation of mouse genetics has been remarkably progressed and provided tools that have greatly facilitated the studies designed to dissect many biological processes in mammalian body, including liver fibrosis. Thus, development of collagen-α1(I)-GFP mice became one of the useful tools to study liver fibrosis [9, 17, 21•, 35••]. Our group has also utilized the collagen-α1(I)-GFP transgenic mouse in which green fluorescent protein (GFP) is upregulated in hepatic myofibroblasts in response to fibrogenic liver injury [36]. These mice can undergo chronic liver injury with repeated CCl_4 injections or BDL to induce liver fibrosis, after which their collagen-producing cells express GFP, which is easily identified by its GFP fluorescence. The expression of collagen-α1(I)-driven GFP in these mice closely correlates with the expression of α-SMA, a general marker for myofibroblasts. The GFP-expressing cells have been considered myofibroblasts [35]. Our strategy to detect hepatic myofibroblasts was based on the investigation of GFP-expressing cells in nonparenchymal fractions of CCl_4-treated or BDL collagen-α1(I)-GFP mice.

The study of the cell fate mapping of HSCs had demonstrated that although there is a decrease in the amount of Vitamin A upon HSC activation, the Vitamin A-specific autofluorescence excited with UV can be still detected in all HSCs by flow cytometry [35, 37]. Whereas the GFP is expressed in all myofibroblasts, the presence of droplets containing of Vitamin A is solely and exclusively attributed to HSC-derived myofibroblasts [35, 37, 38]. To distinguish HSCs from hepatic myofibroblasts of other origins, the flow cytometry has been reported to be a method of choice to distinguish and quantify the contribution of HSCs and portal fibroblasts to liver fibrosis induced by either CCl_4 treatment or BDL. The suggested method used GFP to identify all myofibroblasts. Next, the presence of Vitamin A was used to identify myofibroblasts originated from HSCs, while all other GFP + Vitamin A- myofibroblasts were attributed to myofibroblasts of all other origins. Surprisingly, this GFP + Vitamin A- fraction was composed mostly by Thy1 and TE-1 (elastin) positive cells, while CD45 + Collagen-α1(I)-GFP + fibrocytes [39•] constituted only 4 % of total GFP + fraction. Taken together, the flow cytometry-based quantification analysis of hepatic myofibroblasts activated in fibrotic liver in response to different types of liver injury (toxic and cholestatic) has demonstrated that HSCs are the major source of myofibroblasts in CCl_4-incuced liver fibrosis. However, portal fibroblasts are the major source of myofibroblasts at the onset of BDL-induced liver injury, within a week of BDL. The relative contribution of portal fibroblasts decreases upon chronic cholestatic injury, as HSCs become progressively activated and contribute to the myofibroblast population. Remarkably, the phenotype of BDL-activated HSCs has more similarities with BDL-activated portal fibroblasts rather than with CCl_4-activated HSCs, suggesting that portal fibroblasts might affect (or even regulate) activation of HSCs in BDL-injured liver.

This observation was supported by the gene expression array. Both of these cellular populations were isolated from mouse liver by flow cytometry and the gene expression profile was determined for GFP + Vitamin A + and GFP + Vitamin A- populations from CCl_4- and BDL-injured mice. Gene expression profiling and complimentary immunohistochemistry revealed that myofibroblasts

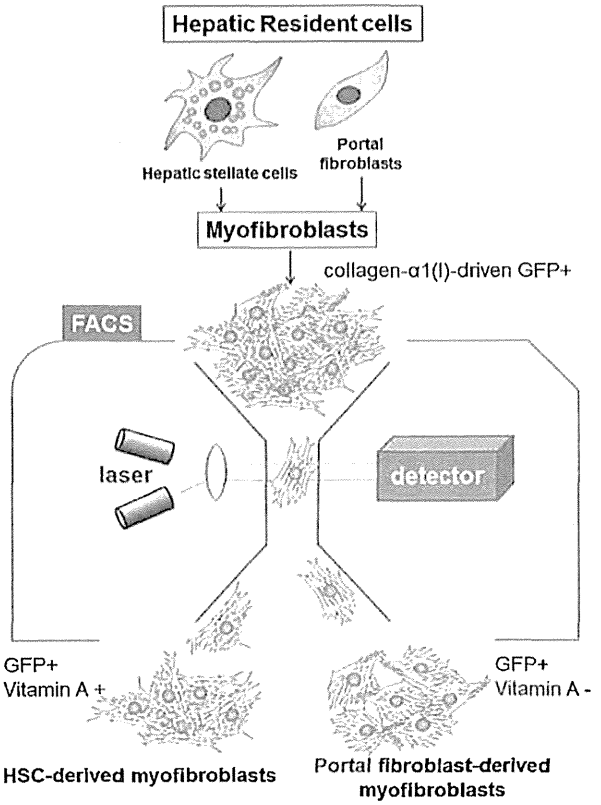

Fig. 1 Strategy to analysis myofibroblasts by flow cytometry: Myofibroblasts expressing collagen-α1(I)-driven GFP+ are identified in nonparenchymal fraction by argon laser at 488 nm wavelength and further fractionated to Vitamin A+ and Vitamin A− cells by UV laser. HSC-derived myofibroblasts are sort-purified as the GFP+ and Vitamin A+ fraction. Portal fibroblast-derived myofibroblasts are sort-purified as the GFP+ and Vitamin A− fraction

derived from HSCs are positive for desmin, and myofibroblasts derived from portal fibroblasts express Thy1, elastin, and mesothelin [35]. Mesothelin is a membrane glycoprotein that is expressed in normal mesothelial cells; however, its function is not clear. In our study, mesothelin was highly expressed in myofibroblasts derived from portal fibroblasts, such that mesothelin may serve as a novel marker of portal fibroblasts. Despite this finding, the function of mesothelin in mice or humans is not yet clear. In addition, recent studies have suggested that liver capsule (which may also express mesothelial markers) can contribute to hepatic myofibroblasts in response to fibrogenic liver injury [7, 40]. At this time, it remains unclear if the mesothelin+ myofibroblasts represent heterogeneous population of hepatic mesenchymal cells that emerge in the damaged liver in response to chronic injury, or is comprised by the same cell type at different stages of activation. Taken together, there might be two major sources of hepatic myofibroblasts in fibrotic liver [39•]. These populations of myofibroblasts may behave similar to each other (Fig. 1), but they exhibit unique properties, and can be distinguished from each other based on their gene expression profile. Therefore, we emphasize that the composition of myofibroblasts varies depending on the etiology of the hepatic injury, and the origin of myofibroblasts may determine the personalized anti-fibrotic therapy of patients with liver fibrosis of different etiologies [35••, 41].

Conclusions

Myofibroblasts are the source of the fibrous scar tissue in liver fibrosis. Hepatic myofibroblasts are transdifferentiated from two main cell populations in response to hepatic injury. The major origins of hepatic myofibroblasts are HSCs and portal fibroblasts. Fibrocytes also contribute to liver fibrosis but their function is not well characterized. Liver fibrosis caused by hepatotoxic injury is attributed to the activated HSCs. However, portal fibroblasts are implicated in liver fibrosis induced by cholestatic liver injury. The contribution of portal fibroblasts to liver fibrosis has not been well characterized because of the difficulties in cell sorting-purification and the lack of identifiable and specific markers for portal fibroblasts. Our novel flow cytometry method makes it possible to distinguish HSC- and portal fibroblast-derived myofibroblasts from the nonparenchymal cell fraction of the fibrotic liver in mice. It is also able to identify a novel specific marker, mesothelin, which is specific to portal fibroblasts. A detailed investigation of myofibroblasts, particularly using new methods such as ours, will provide insight into the mechanisms underlying liver fibrosis, and may lead to the development of more effective therapy.

Compliance with Ethics Guidelines

Conflict of interest Keiko Iwaisako declares a Grant from The Ministry of Education, Culture, Sports, Science and Technology of Japan (No. 26461909), a Grant from Kobayashi Foundation for Cancer Research and a Grant from The Ministry of Health, Labour, and Welfare which are unrelated to this article. Kojiro Taura declares a Grant from The Ministry of Education, Culture, Sports, Science and Technology of Japan (No. 25670575) which is unrelated to this article. Masataka Asagiri declares a Grant from The Ministry of Education, Culture, Sports, Science and Technology of Japan (No. 24659822), a Grant from The Ministry of Education, Culture, Sports, Science and Technology of Japan (No. 24689056) and a Grant from The Ministry of Health, Labour, and Welfare of Japan which are

unrelated to this article. Yukinori Koyama and Kenji Takemoto declare no conflicts of interest.

Human and Animal Rights and Informed Consent This article does not contain any studies with human or animal subjects performed by any of the authors.

References

Papers of particular interest, published recently, have been highlighted as:

- • Of importance
- •• Of major importance

1. Friedman SL (2008) Mechanisms of hepatic fibrogenesis. Gastroenterology 134:1655–1669. doi:10.1053/j.gastro.2008.03.003
2. Zhang DY, Friedman SL (2012) Fibrosis-dependent mechanisms of hepatocarcinogenesis. Hepatology 56:769–775. doi:10.1002/hep.25670
3. Murray KF, Carithers RL Jr, AASLD (2005) AASLD practice guidelines: evaluation of the patient for liver transplantation. Hepatology 41:1407–1432
4. Pellicoro A et al (2014) Liver fibrosis and repair: immune regulation of wound healing in a solid organ. Nat Rev Immunol 14:181–194. doi:10.1038/nri3623
5. Friedman SL (1999) The virtuosity of hepatic stellate cells. Gastroenterology 117:1244–1246
6. Lee UE, Friedman SL (2011) Mechanisms of hepatic fibrogenesis. Best Pract Res Clin Gastroenterol 25:195–206. doi:10.1016/j.bpg.2011.02.005
7. Lua I et al (2014) Mesodermal mesenchymal cells give rise to myofibroblasts, but not epithelial cells, in mouse liver injury. Hepatology 60:311–322. doi:10.1002/hep.27035
8. • Brenner DA et al (2012) Origin of myofibroblasts in liver fibrosis. Fibrogenesis Tissue Repair 6:S17. *The authors summarize that the origin of myofibroblasts are different for different types of chronic liver diseases*
9. Taura K et al (2010) Hepatocytes do not undergo epithelial-mesenchymal transition in liver fibrosis in mice. Hepatology 51:1027–1036. doi:10.1002/hep.23368
10. Bataller R, Brenner DA (2005) Liver fibrosis. J Clin Invest 115:109–118
11. Jenne CN, Kubes P (2013) Immune surveillance by the liver. Nat Immunol 14:996–1006. doi:10.1038/ni.2691
12. Liu Y et al (2012) IL-13 signaling in liver fibrogenesis. Front Immunol 3:116. doi:10.3389/fimmu.2012.00116
13. Shi Z, Wakil AE, Rockey DC (1997) Strain-specific differences in mouse hepatic wound healing are mediated by divergent T helper cytokine responses. Proc Natl Acad Sci USA 94:10663–10668
14. Li J et al (2012) Significance of the balance between regulatory T (Treg) and T helper 17 (Th17) cells during hepatitis B virus related liver fibrosis. PLoS One 7:e39307. doi:10.1371/journal.pone.0039307
15. Iredale JP, Thompson A, Henderson NC (2013) Extracellular matrix degradation in liver fibrosis: biochemistry and regulation. Biochim Biophys Acta 1832:876–883. doi:10.1016/j.bbadis.2012.11.002
16. Barry-Hamilton V et al (2010) Allosteric inhibition of lysyl oxidase-like-2 impedes the development of a pathologic microenvironment. Nat Med 16:1009–1017. doi:10.1038/nm.2208
17. Eyden B (2008) The myofibroblast: phenotypic characterization as a prerequisite to understanding its functions in translational medicine. J Cell Mol Med 12:22–37. doi:10.1111/j.1582-4934.2007.00213.x
18. Schürch W et al (1998) The myofibroblast: a quarter century after its discovery. Am J Surg Pathol 22:141–147
19. Scholten D et al (2011) Migration of fibrocytes in fibrogenic liver injury. Am J Pathol 179:189–198. doi:10.1016/j.ajpath.2011.03.049
20. Parola M, Marra F, Pinzani M (2008) Myofibroblast-like cells in liver fibrogenesis: emerging concepts in a rapidly moving scenario. Mol Asp Med 29:58–66
21. • Kisseleva T et al (2012) Myofibroblasts revert to an inactive phenotype during regression of liver fibrosis. Proc Natl Acad Sci USA 109:9448–9453. doi: 10.1073/pnas.1201840109. *This study by using genetic labeling of aHSCs/myofibroblasts demonstrates that some aHSCs escape cell death and revert to an inactivated phenotype*
22. Troeger JS et al (2012) Deactivation of hepatic stellate cells during liver fibrosis resolution in mice. Gastroenterology 143(1073–83):e22. doi:10.1053/j.gastro.2012.06.036
23. Shi J et al (1998) Evidence of hepatocyte apoptosis in rat liver after the administration of carbon tetrachloride. Am J Pathol 153:515–525
24. Ljubuncic P, Tanne Z, Bomzon A (2000) Evidence of a systemic phenomenon for oxidative stress in cholestatic liver disease. Gut 47:710–716
25. Desmet VJ (2011) Ductal plates in hepatic ductular reactions. Hypothesis and implications. I. Types of ductular reaction reconsidered. Virchows Arch 458:251–259. doi:10.1007/s00428-011-1048-3
26. Popov Y et al (2010) Macrophage-mediated phagocytosis of apoptotic cholangiocytes contributes to reversal of experimental biliary fibrosis. Am J Physiol Gastrointest Liver Physiol 298:G323–G334. doi:10.1152/ajpgi.00394.2009
27. Senoo H et al (2010) Hepatic stellate cell (vitamin A-storing cell) and its relative–past, present and future. Cell Biol Int 34:1247–1272. doi:10.1042/CBI20100321
28. Blaner WS et al (2009) Hepatic stellate cell lipid droplets: a specialized lipid droplet for retinoid storage. Biochim Biophys Acta 1791:467–473. doi:10.1016/j.bbalip.2008.11.001
29. Shirakami Y et al (2012) Hepatic metabolism of retinoids and disease associations. Biochim Biophys Acta 1821:124–136. doi:10.1016/j.bbalip.2011.06.023
30. Wells RG (2014) The portal fibroblast: not just a poor man's stellate cell. Gastroenterology 147:41–47. doi:10.1053/j.gastro.2014.05.001
31. Wells RG, Kruglov E, Dranoff JA (2004) Autocrine release of TGF-beta by portal fibroblasts regulates cell growth. FEBS Lett 559:107–110
32. Li Z et al (2007) Transforming growth factor-and substrate stiffness regulate portal fibroblast activation in culture. Hepatology 46:1246–1256
33. Motoyama H et al (2014) Cytoglobin is expressed in hepatic stellate cells, but not in myofibroblasts, in normal and fibrotic human liver. Lab Invest 94:192–207. doi:10.1038/labinvest.2013.135
34. Perepelyuk M et al (2013) Hepatic stellate cells and portal fibroblasts are the major cellular sources of collagens and lysyl oxidases in normal liver and early after injury. Am J Physiol Gastrointest Liver Physiol 304:G605–G614. doi:10.1152/ajpgi.00222.2012
35. •• Iwaisako K et al (2014) Origin of myofibroblasts in the fibrotic liver in mice. Proc Natl Acad Sci USA 29. pii: 201400062. [Epub ahead of print] *This study demonstrates that the novel flow cytometry-based method enables identification of hepatic myofibroblasts and isolation of distinct subsets of myofibroblasts*
36. Yata Y et al (2003) DNase I-hypersensitive sites enhance alpha1(I) collagen gene expression in hepatic stellate cells. Hepatology 37:267–276

37. Mederacke I et al (2013) Fate tracing reveals hepatic stellate cells as dominant contributors to liver fibrosis independent of its actiology. Nat Commun 4:2823. doi:10.1038/ncomms3823
38. Kisseleva T, Brenner DA (2013) Inactivation of myofibroblasts during regression of liver fibrosis. Cell Cycle 12:381–382. doi:10.4161/cc.23549
39. • Kisseleva T, Brenner DA (2012) The phenotypic fate and functional role for bone marrow-derived stem cells in liver fibrosis. J Hepatol 56:965–972. doi: 10.1016/j.jhep.2011.09.021. *The authors summarizes that bone marrow derived cells play an important role in pathogenesis and resolution of liver fibrosis*
40. Li Y et al (2013) Mesothelial cells give rise to hepatic stellate cells and myofibroblasts via mesothelial-mesenchymal transition in liver injury. Proc Natl Acad Sci USA 110:2324–2329. doi:10.1073/pnas.1214136110
41. Kisseleva T, Brenner DA (2011) Anti-fibrogenic strategies and the regression of fibrosis. Best Pract Res Clin Gastroenterol 25:305–317. doi:10.1016/j.bpg.2011.02.011

PNAS PLUS

Origin of myofibroblasts in the fibrotic liver in mice

Keiko Iwaisako[a,b,c,1], Chunyan Jiang[a,c,d,1], Mingjun Zhang[a,1], Min Cong[a,c,d], Thomas Joseph Moore-Morris[e], Tae Jun Park[a], Xiao Liu[a,c], Jun Xu[a,c], Ping Wang[a,c,d], Yong-Han Paik[f], Fanli Meng[a,g], Masataka Asagiri[h], Lynne A. Murray[i], Alan F. Hofmann[a], Takashi Iida[j], Christopher K. Glass[k], David A. Brenner[a], and Tatiana Kisseleva[c,2]

Departments of [a]Medicine, [c]Surgery, and [k]Cellular and Molecular Medicine, and [e]School of Pharmacy, University of California, San Diego, La Jolla, CA 92093; [b]Department of Target Therapy Oncology, Graduate School of Medicine, Kyoto University, Kyoto 606-8507, Japan; [d]Beijing Friendship Hospital, Capital Medical University, Beijing 100050, China; [f]Division of Gastroenterology and Hepatology, Department of Internal Medicine, Samsung Medical Center, Sungkyunkwan University School of Medicine, Seoul 135-710, Korea; [g]Department of Hepatology, Qilu Hospital Shandong University, Shandong 250012, China; [h]Innovation Center for Immunoregulation and Therapeutics, Graduate School of Medicine, Kyoto University, Kyoto 606-8507, Japan; [i]MedImmune Ltd., Cambridge CB21 6GH, United Kingdom; and [j]Department of Chemistry, College of Humanities and Sciences, Nihon University, Sakurajousui, Setagaya, Tokyo 156-8550, Japan

Edited* by Michael Karin, University of California, San Diego School of Medicine, La Jolla, CA, and approved June 23, 2014 (received for review January 6, 2014)

Hepatic myofibroblasts are activated in response to chronic liver injury of any etiology to produce a fibrous scar. Despite extensive studies, the origin of myofibroblasts in different types of fibrotic liver diseases is unresolved. To identify distinct populations of myofibroblasts and quantify their contribution to hepatic fibrosis of two different etiologies, collagen-α1(I)-GFP mice were subjected to hepatotoxic (carbon tetrachloride; CCl_4) or cholestatic (bile duct ligation; BDL) liver injury. All myofibroblasts were purified by flow cytometry of GFP$^+$ cells and then different subsets identified by phenotyping. Liver resident activated hepatic stellate cells (aHSCs) and activated portal fibroblasts (aPFs) are the major source (>95%) of fibrogenic myofibroblasts in these models of liver fibrosis in mice. As previously reported using other methodologies, hepatic stellate cells (HSCs) are the major source of myofibroblasts (>87%) in CCl_4 liver injury. However, aPFs are a major source of myofibroblasts in cholestatic liver injury, contributing >70% of myofibroblasts at the onset of injury (5 d BDL). The relative contribution of aPFs decreases with progressive injury, as HSCs become activated and contribute to the myofibroblast population (14 and 20 d BDL). Unlike aHSCs, aPFs respond to stimulation with taurocholic acid and IL-25 by induction of collagen-α1(I) and IL-13, respectively. Furthermore, BDL-activated PFs express high levels of collagen type I and provide stimulatory signals to HSCs. Gene expression analysis identified several novel markers of aPFs, including a mesothelial-specific marker mesothelin. PFs may play a critical role in the pathogenesis of cholestatic liver fibrosis and, therefore, serve as an attractive target for antifibrotic therapy.

ECM deposition | markers of fibrogenic myofibroblasts

Chronic liver injury of many etiologies results in liver fibrosis. There are two general types of chronic liver diseases, hepatocellular (injury to hepatocytes, such as chronic viral hepatitis and nonalcoholic steatohepatitis) and cholestatic (obstruction to bile flow, such as primary biliary cirrhosis and primary sclerosing cholangitis) (1). Experimental rodent models of liver fibrosis mimic these two types of chronic liver injuries: Repeated carbon tetrachloride (CCl_4) administration produces hepatocelluar injury, and common bile duct ligation (BDL) produces cholestatic injury (2). In all chronic liver diseases, myofibroblasts are embedded in the fibrous scar and are the source of this excessive extracellular matrix (ECM). Myofibroblasts, which are not present in normal liver, are characterized by distinct morphology, contractility with intracellular stress fibers [α-smooth muscle actin (α-SMA), nonmuscle myosin, and vimentin], and secretion of extracellular matrix (fibronectin and fibrillar collagens) (1, 2).

The cells of origin of hepatic myofibroblasts are unresolved, and perhaps the fibrosis induced by different types of liver injury results from different fibrogenic cells. Hepatic myofibroblasts may originate from bone marrow (BM)-derived mesenchymal cells and fibrocytes, but only a small contribution of BM-derived cells to the myofibroblast population has been detected in experimental liver fibrosis (3–5). Another potential source of myofibroblast is epithelial-to-mesenchymal transition (EMT), in which epithelial cells acquire a mesenchymal phenotype and may give rise to fully differentiated myofibroblasts. However, recent cell fate mapping studies have failed to detect any hepatic myofibroblasts originating from hepatocytes, cholangiocytes, or epithelial progenitor cells (3, 6–10). Thus, the major sources of myofibroblasts in liver fibrosis are the endogenous liver mesenchymal cells, which consist of portal fibroblasts and hepatic stellate cells.

Quiescent hepatic stellate cells (qHSCs) are located in the space of Disse, store retinoids in lipid droplets, and express neural markers, such as glial fibrillary acidic protein (GFAP), synaptophisin, and nerve growth factor receptor p75 (1). In response to injury, qHSCs down-regulate vitamin A-containing lipid droplets and neural markers, and differentiate into α-SMA–expressing myofibroblasts (1, 2). Portal fibroblasts normally comprise a small population of the fibroblastic cells that surround the portal vein to maintain integrity of portal tract. They were first described as "mesenchymal cells not related to sinusoids," and since then have been called "periductular fibroblasts" or portal/periportal mesenchymal cells" (11) and implicated by association in the pathogenesis of cholestatic liver injury. In

Significance

Liver resident activated hepatic stellate cells (aHSCs), and activated portal fibroblasts (aPFs) are the major source of the fibrous scar in the liver. aPFs have been implicated in liver fibrosis caused by cholestatic liver injury, whereas fibrosis in hepatotoxic liver injury is attributed to aHSCs. However, the contribution of aPFs to cholestatic fibrosis is not well characterized because of difficulties in cell purification and the lack of identified aPF-specific markers. We have developed a novel flow cytometry-based method of aPFs purification from the nonparenchymal cell fraction of collagen-α1(I)-GFP mice and have identified potential aPF-specific markers. The goal of this study is to determine whether aPFs contribute to cholestatic liver fibrosis and identify the mechanism(s) of their activation.

Author contributions: K.I., C.J., M.Z., D.A.B., and T.K. designed research; K.I., C.J., M.Z., M.C., T.J.M.-M., T.J.P., X.L., J.X., P.W., Y.-H.P., F.M., L.A.M., and T.K. performed research; M.A., A.F.H., T.I., C.K.G., and D.A.B. contributed new reagents/analytic tools; K.I., C.J., M.Z., M.C., T.J.M.-M., T.J.P., X.L., J.X., Y.-H.P., F.M., M.A., and C.K.G. analyzed data; and D.A.B. and T.K. wrote the paper.

The authors declare no conflict of interest.

*This Direct Submission article had a prearranged editor.

Freely available online through the PNAS open access option.

[1]K.I., C.J., and M.Z. contributed equally to this work.

[2]To whom correspondence should be addressed. Email: tkisseleva@ucsd.edu.

This article contains supporting information online at www.pnas.org/lookup/suppl/doi:10.1073/pnas.1400062111/-/DCSupplemental.

response to chronic injury, portal fibroblasts may proliferate, differentiate into α-SMA–expressing myofibroblasts, and synthesize extracellular matrix (11–14).

The contribution of portal fibroblasts (PFs) to liver fibrosis of different etiologies is not well understood, mainly because of difficulties in isolating PFs and myofibroblasts. The most widely used method of PF isolation from rats is based on liver perfusion with enzymatic digestion followed by size selection (15). Cell outgrowth from dissected bile segments is still used to isolate mouse PFs, and after 10–14 d in culture, PFs undergo progressive myofibroblastic activation (16). The disadvantage of this technique is that it requires multiple passaging and prolong culturing (11). A more physiological method of PF culturing in a precision-cut liver slice is designed to maintain cell–cell and cell–matrix interactions and mimic natural microenvironment of PFs, but it does not enable the study of purified PFs (17). Therefore, only a few markers of PFs are available to identify PFs in the myofibroblast population, including gremlin, Thy1, fibulin 2, interleukin 6 (IL-6), elastin, the ecto-AT-Pase nucleoside triphosphate diphosphohydrolase-2 (NTPD2), and coffilin 1. In addition, the lack of desmin, cytoglobin, α2-macroglobulin, neural proteins (GFAP, p75, synaptophysin), and lipid droplets distinguishes PFs from HSCs (1, 17–21).

Our study uses transgenic reporter mice and new flow cytometry protocols to identify the origin of myofibroblasts and quantify their numbers in two murine models of chronic liver injury (BDL and CCl_4). Our study demonstrates that the origin of the myofibroblasts is determined by the type of liver injury. As previously reported using other methodologies, HSCs are the major source of myofibroblasts in CCl_4 liver injury. In contrast, most of the myofibroblasts at the onset of BDL-induced liver injury originate from activated PFs (aPFs).

Results

BDL- and CCl_4-Induced Liver Fibrosis Is Associated with Activation of Myofibroblasts in Mice. To study activation of hepatic myofibroblasts, Col-GFP mice expressing GFP under control of collagen α1(I) promoter/enhancer (22) were subjected to BDL (20 d) or CCl_4 (1.5 mo) liver injury. Upon activation, hepatic myofibroblasts in these mice are visualized by GFP expression. Development of liver fibrosis was confirmed in Col-GFP mice by hydroxyproline content, Sirius Red staining (Fig. 1 *A* and *B*) and correlated with increased collagen-α1(I) (fold increase 6.1 ± 0.3 and 7.6 ± 0.4 in BDL- and CCl_4-treated vs. control mice) and α-SMA mRNA expression (fold increase 4.2 ± 0.2 and 6.1 ± 0.7 vs. control mice, respectively; Fig. 1*B*). Development of liver fibrosis was also associated with activation of myofibroblasts, demonstrated by Col-GFP expression (6.5 ± 0.4% and 7.8 ± 0.5% of GFP^+ area in BDL- and CCl_4-treated vs. 0.3 ± 0.03% in control mice) and α-SMA expression (Fig. 1*B*). Thus, BDL and CCl_4 induced comparable levels of fibrosis and activation of myofibroblasts in the liver, sufficient to isolate GFP^+ myofibroblasts and determine their composition in response to two different injuries.

Isolation of Myofibroblasts. The reporter Col-GFP mice (22) have been extensively characterized and are widely used to visualize activated myofibroblasts in fibrotic liver, lungs, kidneys, and skin (3–5, 8, 23–36). Expression of GFP in these mice closely correlates with expression of collagen type I protein in hepatic myofibroblasts but is not expressed in endothelial, epithelial, or other cell types (37–39). Using Col-GFP mice we have demonstrated that activated hepatic stellate cells (aHSCs) (GFP^+, vitamin A^+, $Desmin^+$ cells) comprise >92% of myofibroblasts in response to CCl_4-induced or alcohol-induced fibrosis (1, 40).

Analysis of Activated Myofibroblasts by Flow Cytometry. Our strategy to determine the composition of hepatic myofibroblasts is based on characterization of GFP^+ cells in nonparenchymal liver fractions of BDL- and CCl_4-treated Col-GFP mice (which contains all $Col1a1^+$ and $\alpha\text{-}SMA^+$ myofibroblasts; for details, see Fig. S1*A*) (22). Although collagen-α1(I)-GFP is expressed in all activated myofibroblasts (40, 41), expression of vitamin A (Vit.A) droplets in the liver is solely attributed to HSCs (1) (Fig. 2*A*). The cell fate mapping of HSCs [using $GFAP^{Cre}$ × $Rosa26^{flox\text{-}TmRed\text{-}Stop\text{-}flox\text{-}GFP}$ mice (40); Fig. S1 *B* and *C*] demonstrated that although HSCs down-regulate vitamin A upon activation (aHSCs), vitamin A is still detected in all aHSCs by flow cytometry (autofluorescent signal of vitamin A; Fig. S1*D*). We used flow cytometry to quantify the contribution of aHSCs ($GFP^+Vit.A^+$) and myofibroblasts of other origins ($GFP^+Vit.A^-$) in BDL and CCl_4 injury (Fig. 2*B*). As expected, activation of hepatic myofibroblasts (GFP^+ cells, 100%) was observed only in injured livers (Fig. 2*B*). CCl_4-activated myofibroblasts contained 87 ± 6% $GFP^+Vit.A^+$ and 13 ± 3% $GFP^+Vit.A^-$ cells. In contrast, the nonparenchymal fraction from BDL (20 d) mice consisted of 56 ± 4% $GFP^+Vit.A^+$ and 42 ± 5% $GFP^+Vit.A^-$ myofibroblasts, suggesting that the composition of GFP^+

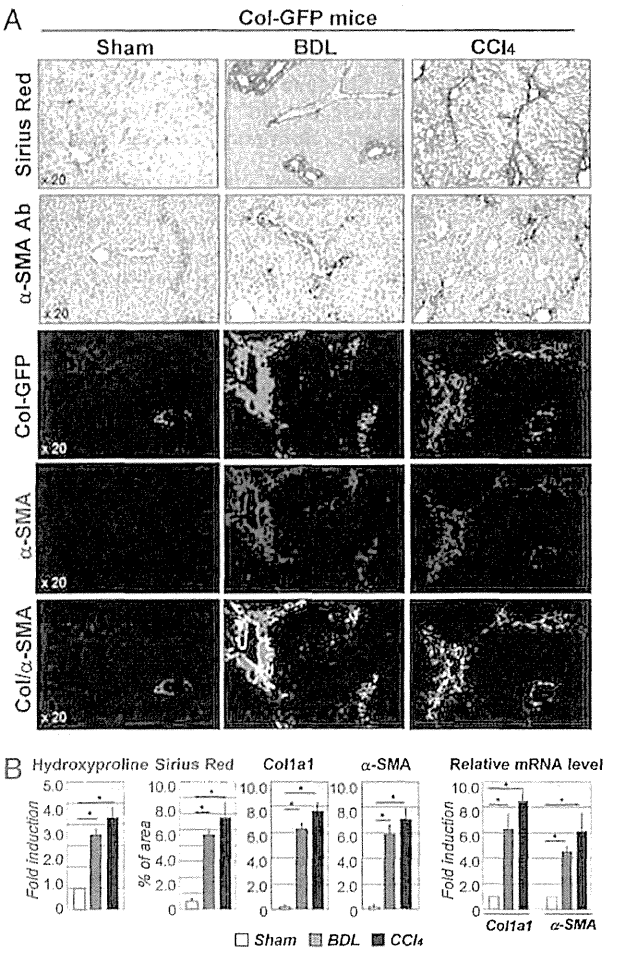

Fig. 1. Development of liver fibrosis in Col-GFP mice in response to BDL and CCl_4. (*A*) CCl_4-treated and BDL-operated mice (but not sham mice, 8-wk-old, $n = 10$ per group) developed liver fibrosis, as shown by Sirius Red staining, fluorescent microscopy for collagen-GFP, and staining for α-SMA (20× objective). (*B*) Fibrosis was assessed by hydroxyproline and Sirius Red (positive area) content and by mRNA levels of fibrogenic genes (Col and α-SMA) in all groups of mice is shown, $^*P < 0.003$; $^{**}P < 0.001$.

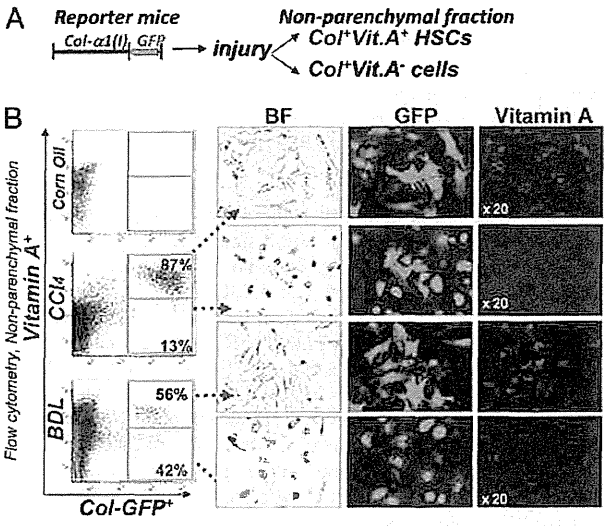

C

GFP⁺ Myofibroblasts, %		Vit.A⁺	Vit.A⁻
CCl_4	5 days	79 ± 3.8	5 ± 2.0
CCl_4	14 days	88 ± 4.0	10 ± 3.6
CCl_4	1.5 mo	87 ± 5.2	13 ± 2.0
BDL	5 days	18 ± 7	73 ± 5
BDL	17 days	45 ± 3	53 ± 4
BDL	20 days	56 ± 4	46 ± 3

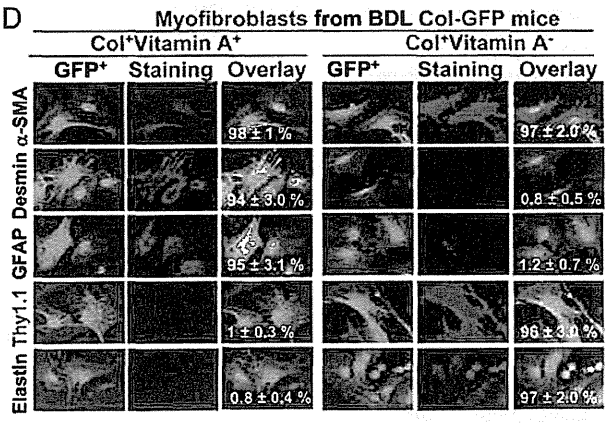

E

GFP⁺ Myofibroblasts, %		HSCs	aPFs	Others
CCl_4	1.5 mo	83 ± 5.2	13 ± 2.0	4 ± 2.4
BDL	5 day	18 ± 7	73 ± 5	3 ± 2
BDL	17 days	47 ± 3	49 ± 6	4 ± 0.8
BDL	20 days	51 ± 4	43 ± 3	3 ± 1.4

Fig. 2. Detection, quantification, and isolation of liver myofibroblasts. (*A*) Strategy to analyze myofibroblasts by flow cytometry: Collagen type I-expressing myofibroblasts were identified in nonparenchymal fraction by GFP expression and further fractionated to Vit.A$^+$ and Vit.A$^-$ cells. (*B*) FACS analysis of nonparenchymal fraction from untreated and BDL-, and CCl_4-treated Col-GFP mice: GFP$^+$ cells were detected by argon laser at 488 nm wavelength, and Vit.A$^+$ cells were detected by violet laser at 405 nm wavelength. Representative dot plots are shown, $P < 0.03$. GFP$^+$Vit.A$^+$ and GFP$^+$Vit.A$^-$ cells were sort purified and analyzed by light and fluorescent microscopy for GFP and Vitamin A expression (UV laser, 20× objective). (*C*) Flow cytometry-based quantification of GFP$^+$ myofibroblasts. Expression of vitamin A in GFP$^+$ cells was analyzed in nonparenchymal fraction of Col-GFP mice at different time points ($n = 6$ per time point) of CCl_4 and BDL, $P < 0.01$. (*D*) Immunophenotyping of GFP$^+$ myofibroblasts isolated from BDL mice. GFP$^+$Vit.A$^+$ and GFP$^-$Vit.A$^-$ fractions were sort purified from Col-GFP mice ($n = 6$) after BDL (20 d). Expression of myofibroblast marker (α-SMA), HSC markers (desmin, GFAP, CD146), and PF markers (elastin, Thy1) were analyzed by immunocytochemistry using specific antibodies or isotype matched controls (40× objective). GFP$^+$Vit.A$^+$ and GFP$^+$Vit.A$^-$ cells were identified as aHSCs and aPFs, respectively. For each fraction, the percent of positively stained cells is calculated (compared with total cells, 100%, $P < 0.05$). (*E*) Quantification of GFP$^+$Vit.A$^+$ and GFP$^+$Vit.A$^-$ fractions is based on expression of HSC- and PF-specific markers in GFP$^+$ myofibroblasts (100%) as detected by immunocytochemistry, $P < 0.05$.

myofibroblasts varies depending on the etiology of liver fibrosis. GFP$^+$Vit.A$^+$ and GFP$^+$Vit.A$^-$ cells were sort purified and plated (Fig. 2*B*). Expression of GFP was confirmed in both fractions by fluorescent microscopy, whereas expression of Vit.A$^+$ droplets was detected only in GFP$^+$Vit.A$^+$ cells.

Activation of HSCs Differs in BDL- and CCl_4-Induced Liver Injury. Analysis of all GFP$^+$ myofibroblasts (100%) demonstrated that GFP$^+$Vit.A$^+$ aHSCs are the major source of activated myofibroblasts in response to CCl_4 liver injury (Fig. 2*B*). Even at earlier time points of CCl_4 treatment, 79 ± 3% (at 5 d) and 88 ± 4% (at 14 d) of the myofibroblasts were GFP$^+$Vit.A$^+$ HSCs (Fig. S2*A*). In contrast, BDL activated fewer HSCs (Fig. S2*B*). After 5 d of BDL, GFP$^+$ myofibroblasts were mainly composed by GFP$^+$ Vit.A$^-$ cells (73 ± 5%), whereas GFP$^+$Vit.A$^+$ aHSCs represented only 18 ± 7% of GFP$^+$ cells. After BDL (17 d), GFP$^+$ myofibroblasts consisted of 53 ± 4% of GFP$^+$Vit.A$^-$ cells and 45 ± 3% of GFP$^+$Vit.A$^+$ aHSCs, suggesting that activation of HSCs in BDL follows the induction of GFP$^+$Vit.A$^-$ myofibroblasts. Flow cytomery-based statistical analysis of the number of Vit.A$^+$ and Vit.A$^-$ myofibroblasts in response to BDL and CCl_4 is summarized in Fig. 2*C*.

GFP$^+$Vit.A$^+$ Myofibroblast Originate from HSCs, Whereas GFP$^+$Vit.A$^-$ Derive Predominantly from aPFs. Sort-purified GFP$^+$Vit.A$^-$ and GFP$^+$Vit.A$^+$ myofibroblasts were characterized by immunostaining for specific markers. As expected, all GFP$^+$ cells expressed the myofibroblast marker α-SMA, demonstrating that only myofibroblasts express type I collagen in liver fibrosis. BDL-activated GFP$^+$Vit.A$^+$ myofibroblasts expressed the typical HSC markers GFAP (94 ± 2.6%), desmin (98 ± 2%), and mesenchymal marker CD146 (87 ± 3.0%), confirming that the GFP$^+$ Vit.A$^+$ fraction consists solely of aHSCs (Fig. 2*D*). As expected, CCl_4-induced GFP$^+$Vit.A$^+$ myofibroblasts were aHSCs (Fig. S3*A*). In contrast, GFP$^+$Vit.A$^-$ myofibroblasts stained positive for the established portal fibroblast markers Thy1 (93 ± 4.0%) and elastin (86 ± 3.4%), but lacked markers of HSCs (GFAP, Desmin, CD146; Fig. 2*D*) and myeloid cells (CD11b, F4/80, CD68; Fig. S3*B*). Only a small number of GFP$^+$Vit.A$^-$ cells expressed fibrocyte-like markers CD45 (3.1 ± 0.1%) and CD11b (2.4 ± 0.3%; Fig. S3*B*), suggesting that GFP$^+$Vit.A$^-$ fraction predominantly (95 ± 4%) contains aPFs, and that less than 4 ± 1% of myofibroblasts originate from other sources (e.g., fibrocytes and BM derived mesenchymal progenitors). Immunocytochemistry-based analysis of myofibroblast composition in response to both BDL and CCl_4 is summarized in Fig. 2*E*.

Gene Expression Profile Distinguishes BDL-Derived aPFs from CCl_4-aHSCs and BDL-aHSCs. The gene expression profile of BDL-aPFs was compared with BDL-aHSCs and CCl_4-aHSCs (Fig. 3*A*). Using a threshold defining confident detection of gene expression, we confirmed that aPFs exhibited a myofibroblast-like phenotype, sharing mRNA expression of 8,981 genes with aHSCs. These genes included *Col1a1*, *Col1a2*, *Col2a1*, *TIMP-1*, *Spp1*, *TGFβ-RI*, and *Vimentin* (Fig. 3*C*) and were induced in aPFs to a level comparable to BDL- and CCl_4-aHSCs. As expected, GFAP and Bambi mRNAs were highly expressed in

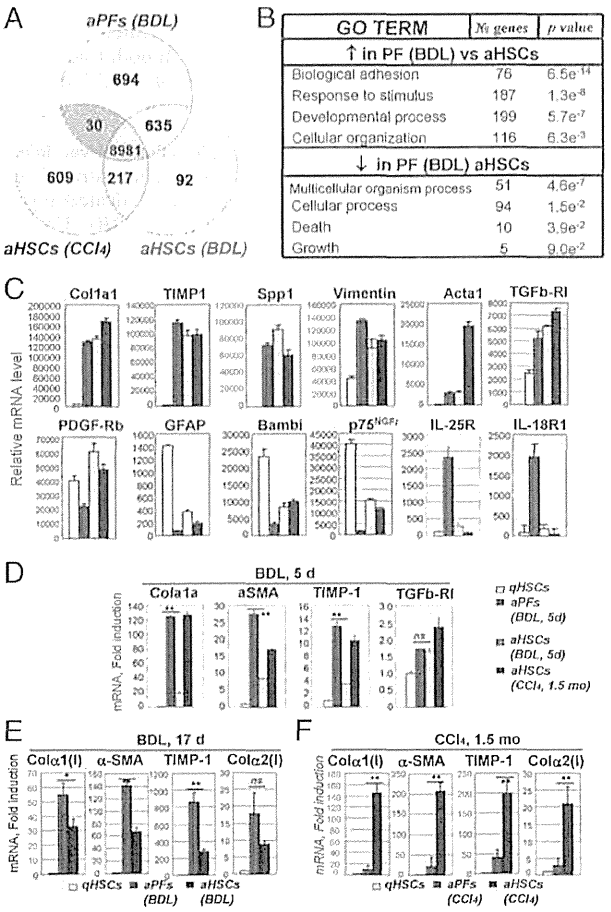

Fig. 3. Characterization of aPFs and aHSCs. (*A*) BDL (20 d) GFP$^+$Vit.A$^-$ aPFs and GFP$^+$Vit.A$^+$ aHSCs were analyzed by the whole mouse genome microarray, and their gene expression profile was compared with that in CCl_4-activated GFP$^+$Vit.A$^+$ HSCs. Venn diagrams of the cell group-enriched genes that exhibited more than a twofold up-regulation compared with other groups. (*B*) GO TERM: demonstrates the signaling pathways that were up-regulated or down-regulated in BDL-aPFs versus BDL- or CCl_4-aHSCs. (*C*) Expression of selected genes in qHSCs, BDL-aHSCs and BDL-aPFs, and CCl_4-aHSCs. The results are relative mRNA level (average of normalized values/multiple probes/per gene) obtained by Agilant microarray, $P < 0.001$. (*D*) Expression of fibrogenic genes was analyzed by RT-PCR in BDL- (5 d) aPFs and BDL-aHSCs, isolated from the same mice ($n = 6$), and compared with that in qHSCs-aHSCs and CCl_4 (1.5 mo)-aHSCs. The data are shown as fold induction compared with qHSCs, $^{**}P < 0.02$ is shown for BDL-aPFs and BDL-aHSCs; ns is not significant. (*E*) Expression of fibrogenic genes was analyzed in BDL (17 d)-aPFs and BDL-aHSCs (isolated from the same mice, $n = 6$) by RT-PCR vs. qHSCs. The data are shown as fold induction compared with qHSCs, $^{*}P < 0.05$; $^{**}P < 0.01$; ns, nonsignificant. (*F*) Similarly, CCl_4- (1.5 mo)aPFs and CCl_4-aHSCs, isolated from the same mice ($n = 4$) were analyzed by RT-PCR. The data are shown as fold induction over qHSCs, $^{*}P < 0.05$; $^{**}P < 0.01$. The data in *D–F* represent at least three independent experiments.

qHSCs, whereas *PDGF-Rb* was up-regulated in aHSCs. Meanwhile, the highest expression of *Acta1* was detected in CCl_4-aHSCs (Fig. 3*C*). aPFs up-regulated an additional 694 unique genes (Fig. 3*A*). This set of genes was enriched in Gene Ontology biological process annotations linked to biological adhesion, response to stimulus, developmental process and cellular organization (Fig. 3*B*), locomotion, focal adhesion, cell adhesion molecules, regulation of actin cytoskeleton, and were associated with the induction of the profibrogenic Wnt signaling pathway (Fig. S4). Furthermore, aPFs up-regulated expression of IL-18R, IL-25R (Fig. 3*C*), and other genes that distinguish them from aHSCs (Table 1, discussed below). Interestingly, BDL-aHSCs differentially expressed only 92 genes and shared more similarity with aPFs (635 genes) than with CCl_4-aHSCs (217 genes; Fig. 3*A*), suggesting that in response to cholestatic liver injury, aHSCs may mimic the phenotype of aPFs (for comparison of BDL- and CCl_4-aHSCs, see Fig. S5).

PFs Are Activated in Early BDL-Induced Liver Injury. Our data indicate that aPFs and aHSCs exhibit similar level of activation in response to BDL (20 d; Fig. 3*C*). To further characterize the fibrogenic properties of aPF and aHSC, earlier time points of BDL were examined. After 5 d of BDL (Fig. 3*D*), expression levels of *Col1a1*, *aSMA*, and *TIMP1* mRNA were much higher in aPFs than in aHSCs, suggesting that the activation of PF precedes the activation of HSCs in BDL injury. For example, *Col1a1* was 120-fold induced in aPFs over the level in qHSCs, compared with 20-fold induction in aHSCs. After 17 d of BDL (Fig. 3*E*), activation of HSCs became more prominent (i.e., *Col1a1* mRNA: 33-fold induction in aHSCs, vs. 55 in aPFs). Meanwhile, CCl_4-aPFs exhibited a much lower level of *Col1a1* mRNA than CCl_4-aHSCs (fold induction 20 and 160, respectively; Fig. 3*F*), demonstrating that PFs are only minor contributors to toxic CCl_4-induced liver injury. These data are in concordance with our previous results obtained by flow cytometry (Fig. 2) and

Table 1. Expression of signature genes distinguishes BDL-aPFs from BDL- and CCl_4-aHSCs

Maximum induction (up-regulation) in aPF (BDL, 20 d)	Fold
Calcitonin α (Calca)	66
Glycoprotein m6a (Gpm6a)	35
Uroplakin 1β	28
Basonuclin 1 (Bnc1)	24
Mesothelin (msln)	24
Frizzled-related protein 4 (Sfrp4)	21
Cyp2s1	20
Proteoglycan 4 (Prg4)	18
Asporin (aspn)	18
Mucin 16 (Muc16)	16
IL-18R1	14
Myosin light peptide7 (Myl7)	14
Vitrin (Vit)	12
Glipican 3 (Gpc3)	12
CD200	11
Apolipoprotein D (ApoD)	10
IL-25R	9.7
Dermokin (Dmkn)	9.3
Vanin (Vnn1)	8.5
Thrombospondin 4 (Thbs4)	7.0
Integrin β4 (Itgb4)	6.5
CD55	5.6
Gremlin 1 (Grem1)	4.8
NTPD2	4.6
PDGFc	4.6
Fibulin 2 (Fbln2)	4.4
CD9	3.1
Elastin (Eln)	2.3
Thy1 (CD90)	1.8
Cytoglobin	0.6

Using the whole mouse genome microarray, expression of signature genes was determined for BDL-aPFs. Expression of genes previously identified as PF-specific (underlined) was confirmed. Fold induction (compared with the highest value observed in BDL- or CCl_4-aHSCs) is shown for each gene. Full list of genes is shown in Fig. S7.

demonstrate that there is a correlation between increased number of BDL-aPFs and the level of their activation.

Functional Properties of BDL-Derived aPFs Differ from aHSCs. Previous studies have proposed differences in aPFs and aHSCs that underlie fibrogenesis of different etiologies (42). Therefore, we assessed how aPFs and aHSCs responded to fibrogenic stimuli in vitro. As expected, the fibrogenic cytokine TGF-β1 had similar effects on aPF and aHSC (Fig. 4*A*). However, aPFs were unresponsive to the known HSC agonists PDGF and NGF (demonstrated by mRNA expression of target genes *CyclinD1*; *Bax*, *Bid*, *Bim*, *Bcl-2*, and *Bcl-xl*, respectively). Despite high expression of IL-18R, treatment of aPFs with IL-18 (100 ng/mL; 8 h) did not induce expression of tested IL-18 target genes (*MMP3, MMP8*, and *MMP13, Cox-2, iNOS, IL-6*). Meanwhile, only PFs responded to the bile acid TCA, with increased *Col1a1* mRNA expression (>2.2-fold induction over control aPFs), suggesting that TCA may directly mediate PF activation (Fig. 4*B*). Furthermore, aPFs responded to IL-25 stimulation by induction of IL-13 [similar to IL-13 induction by IL-25–treated macrophages (43) and fibroblasts (44)]. Although IL-13 is implicated in HSC activation, and IL-13 levels are up-regulated in patients with liver cirrhosis (3, 4, 27), the role of IL-13 in cholestatic liver injury has not been well defined. We hypothesize that IL-25–mediated IL-13 production by BDL-aPFs may stimulate activation of HSCs. To assess the effect of aPF-produced IL-13 on HSCs, qHSCs were incubated in the presence of IL-13. As we predicted (45), IL-13 increased *CTCF* (after 4 h) mRNA expression, and also induced up-regulation of *Col1a1*, *aSMA*, *TIMP1*, and mRNA (after 24 h) in HSCs (Fig. 4*C*), suggesting that aPFs may locally facilitate HSC activation via production of IL-13. A more detailed analysis (Fig. 4*D*) demonstrated that stimulation of HSCs with IL-13 causes up-regulation of IL-13Ra2 expression (but not IL-13Ra1 or IL-4) and transcription of IL-13 target genes *Tenascin-C* and *Eotaxin* (46, 47). Because IL-13–treated HSCs did not express IL-13 or IL-6, we concluded that IL-13 directly mediated HSC activation, and this effect was associated with phosphorylation of ERK1/2 (which is completely blocked by ERK inhibitor U0126; Fig. 4*E*) and activation of the p38 and Smad1/5 signaling pathways. Similar results were obtained in human primary HSCs. hIL-13 induced a dose-dependent secretion of CCL11/eotaxin (Fig. S6*A*) in hHSCs. In a separate experiment, hIL-13 alone (or in combination with TGF-β1) mediated an increase in IL-13Ra2, *Tenascin C*, *Col1a1*, *Col3a1*, *fibronectin*, and *LoxL2* genes (Fig. S6*B*). In turn, TGF-β1 and serum stimulation did not result in IL-13 secretion by hHSCs (Fig. S6*C*), suggesting that aPFs may serve as a source of IL-13 in liver fibrosis.

Expression of Novel Markers Distinguishes BDL-Derived aPFs from BDL-aHSCs and CCl_4-aHSCs. To further distinguish aPFs from aHSCs and other myofibroblasts, we interrogated the whole mouse genome microarray to determine "signature genes" for aPFs (Table 1). In concordance with previous studies, we confirmed that aPFs lack expression of cytoglobin (an HSC marker), but express Thy1, elastin, Gremlin 1, Fibulin 2, and NTPD2 mRNAs (the markers that have been reported to discriminate between aPFs and aHSCs) (2, 11, 17–21). However, expression of cofilin-1 (21) distinguished aPFs from CCl_4-aHSCs, but not from BDL-aHSCs, which limits the usefulness of this marker. Furthermore, aPFs uniquely expressed calcitonin α (fold induction >48 over the highest value in BDL-aHSCs or CCl_4-aHSCs), mesothelin (>28), uroplakin 1β (>22), basonuclin 1 (>18), asporin (>14), proteoglycan 4 (>14), glipican 3 (>12), and CD200 (>11) mRNA (Fig. S7). Up-regulation of these genes specifically in aPFs [but not in quiescent or aHSCs, endothelial cells, Kupffer cells, and hepatocytes (Fig. 5*A* and Fig. S8*A*) or BDL-activated cholangiocytes (Fig. 5*A* and Fig. S8*C*)] was confirmed by RT-PCR and immunohistochemistry, suggesting that these genes may serve as potential novel markers of aPFs. Some of these genes (including *basonuclin 1, glycoprotein m6a, uroplakin 3b and 1b, mesothelin, IL-18R, calcitonin-related peptides,* and *vitrin*) were reported as signature genes of murine hepatic mesothelial (48) and epicardial cells (49) (Fig. S7), supporting the theory that PFs originate from mesothelial cells (50, 51).

The role of most of these genes in liver fibrosis has not been evaluated, with the exception of calcitonin α and mesothelin. Calcitonin α, a calcium metabolism regulating hormone, was implicated in pathogenesis of cholestatic injury, and mice devoid of calcitonin α are more resistant to BDL-induced liver fibrosis (52). In turn, mesothelin, a glycosylphosphatidylinositol-linked glycoprotein, is expressed in hepatic mesothelial cells and malignant mesotheliomas (53) and mediates intracellular adhesion and metastatic spread (54). Mesothelin knockout mice are viable and exhibit no obvious abnormalities (55). Expression of mesothelin was detected only in isolated aPFs but not in other cellular fractions (Fig. 5*A*).

Expression of Mesothelin Is Up-Regulated in aPFs in Response to Injury. We examined the expression of mesothelin in isolated aPFs and aHSCs. Unlike GFP^+GFAP^+ aHSCs, GFP^+ aPFs expressed mesothelin (97 ± 1.7%). $Mesothelin^+$ aPFs coexpressed elastin (detected with TE-7 Ab) and Thy1, and immunostaining with mesothelin colocalized with $Elastin^+Thy1^+$ aPFs (Fig. 5*B* and Fig. S8*B*). Next, expression of mesothelin was evaluated in livers of BDL- and CCl_4-injured mice (Fig. 5*C* and Fig. S8*B*). In concordance with our previous findings, very few $mesothelin^+$ cells were detected in CCl_4-injured livers. In contrast, mesothelin was highly expressed in livers from BDL-injured mice, with an expression pattern similar to the other PF markers Thy1 and elastin (Fig. S8 *B* and *C*). In support of our findings, expression of mesothelin mRNA was also detected in laser capture microdissected portal areas from BDL (20 d)-treated mice but not from CCl_4-treated mice (Fig. 5*D*). In addition, mesothelin was not expressed in sham-operated mice, suggesting that mesothelin identifies the aPF phenotype.

Discussion

Our study was designed to determine the origin of hepatic myofibroblasts activated in response to chronic injury of two different etiologies. We demonstrate that hepatotoxic (CCl_4) and cholestatic (BDL) liver injuries activate distinct subsets of fibrogenic myofibroblasts. Thus, CCl_4 activates preferentially aHSCs, whereas BDL initially preferentially aPFs. We developed a reliable method of isolation and quantification of hepatic myofibroblast fractions by using flow cytometry. Based on the distinctive expression of Vitamin A and GFAP in HSCs and Thy1 and elastin in PFs, this study establishes cell sorting as a robust method to purify distinct populations of myofibroblasts in mice, providing a nonbiased approach to purify and characterize all myofibroblasts. By demonstrating that HSCs are the major source of myofibroblasts in hepatotoxic liver injury (CCl_4), we confirmed the previous cell fate mapping studies that used GFAP-Cre (56, 57), PDGFRb-Cre (58), and Lrat-Cre (59).

In contrast to CCl_4-induced injury, our study demonstrates that PFs rapidly activate at the onset of cholestatic injury and up-regulate fibrogenic genes. Furthermore, early activation of PFs during BDL injury may affect HSCs, and BDL-aHSCs exhibit more similarity to aPFs than to CCl_4-aHSCs. Gene expression profiling demonstrated novel signature genes for aPFs. According to cell fate mapping, PFs originate from the mesothelium (51, 60), and our data suggest that aPFs share similarity in signature gene expression with other cells of mesothelial origin. One of these genes, mesothelin, is highly induced specifically in aPFs in response to BDL injury, suggesting that mesothelin may become a new target for antifibrotic therapy.

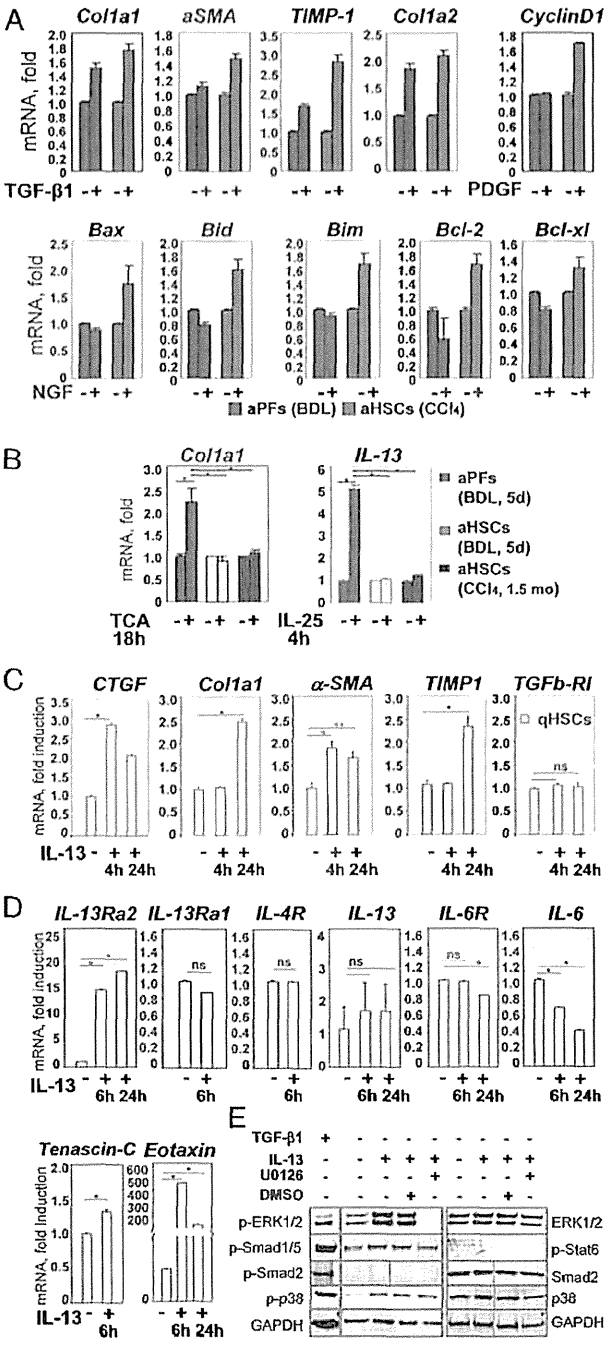

Fig. 4. Functional properties of aPFs and aHSCs. (*A*) Response to cytokines was compared in BDL-aPFs and CCl_4-aHSCs. Both aHSCs and aPFs responded to TGF-β1 (10 ng/mL). aHSCs, but not aPFs, responded to PDGF (100 pg/mL) and NGF (100 ng/mL). The data are fold induction compared with untreated aPFs (or aHSCs), $P < 0.01$. (*B*) BDL-aPFs (but not BDL-aHSCs or CCl_4-aHSCs) responded to bile acid taurocholic acid (TCA; 1,200 nmol/mL) by up-regulation of *Col1a1*, and to IL-25 (100 ng/mL) by IL-13 secretion, $P < 0.05$. Stimulation of aPFs with Tauro-ursodeoxycholate (TUDCA; 25 nmol/mL), deoxycholic acid (DCA; 0.1 nmol/mL), taurochenodeoxycholate (TCDCA; 60 nmol/mL), Tauro b-muricholate (TbMCA; 2,000 nmol/mL), and cholic acid (CA; 20 nmol/mL) did not result in Col1a1 induction. The data are fold induction compared with untreated aPFs (or aHSCs), $^*P < 0.05$. (*C*) The effect of IL-13 on HSC activation was evaluated. qHSCs were incubated with IL-13 (100 ng/mL) for 4 h and 24 h. Gene expression was evaluated by RT-PCR, $^*P < 0.01$; $^{**}P < 0.02$; ns, nonsignificant. The data (*A*–*C*) represent three independent experiments. For each experiment, the cells were isolated from three mice. (*D*) IL-13 signaling in mouse HSCs: IL-13–stimulated HSCs (100 ng/mL, 6 h) up-regulate IL-13Rα2, tenascin C, and eotaxin, but do not express IL-13 or IL-6, as shown by RT-PCR. (*E*) IL-13 signaling in HSCs (2 h) causes phosphorylation of ERK1/2 (which is blocked by ERK inhibitor U0126, 10 μM), p38, and Smad1/5, as shown by Western blot. TGF-β1–stimulated HSCs served as a control.

aHSCs and aPFs Are the Major Source of Myofibroblasts in Fibrotic Liver. Although vitamin A-rich lipid droplets are a distinctive characteristic of HSCs, activation results in a decrease in these droplets (1). However, in vivo aHSCs do not lose their vitamin A droplets completely, and vitamin A-induced buoyancy has become a standard way to purify quiescent and aHSCs in vivo, as confirmed by gene expression profiling (25, 41). Our current study provides additional proof that vitamin A is a reliable marker for identification, quantification, and purification of aHSCs, making flow cytometry using vitamin A autofluorescence as the method of choice to purify aHSCs from myofibroblasts of other origins. Flow cytometry enables identification of hepatic myofibroblasts and isolation of distinct subsets of myofibroblasts (HSCs and PFs) with high purity from the same mouse liver.

Using collagen-GFP reporter mice, we demonstrate that the total population of GFP^+ myofibroblasts isolated in the nonparenchymal fraction consists of two major populations: $Vit.A^+$ aHSCs and $Vit.A^-$ aPFs. These results were confirmed by immunostaining for cell-specific markers, RT-PCR, and gene expression microarrays. Specifically, aHSCs were identified as $Vit.A^+$, $GFAP^+$, $Desmin^+$, and $CD146^+$ cells that exhibit specific morphology. In turn, $Vit.A^-$ aPFs lacked GFAP or Desmin expression, but were characterized by expression of Thy1 and Elastin, and a more round-shaped morphology. Collectively, HSCs and PFs contribute to more than 94% of GFP^+ myofibroblasts. This type of analysis should now be extended to other experimental models of liver fibrosis, such as alcohol-induced liver disease and nonalcoholic steatohepatitis.

aHSCs and aPFs Contribute Differently to Liver Fibrosis of Different Etiologies. Although the role of aPFs in the development of portal fibrosis has been discussed (42, 61), our study is the first to our knowledge to quantify the myofibroblast populations over a time course. Consistent with previous studies (62, 63), we demonstrate that aPFs play an important role at early stages of BDL-induced liver fibrosis (13) by contributing >70% of myofibroblasts. Moreover, even at later stages (BDL, 17–20 d), aPFs contribute ~50% of myofibroblasts and exhibit a more activated phenotype than aHSCs. Thus, the composition of myofibroblasts varies depending on the etiology and time course of liver injury and fibrosis.

Cholestatic Injury Induces Predominant Activation of aPFs. The mechanism of fibrogenesis differs in CCl_4 and BDL models of liver injury. Treatment with CCl_4 is hepatotoxic, causing necrosis of hepatocytes and inflammation in the pericentrolobular area. However, BDL induces obstruction of bile flow with increased biliary pressure, moderate inflammation, and cytokine secretion by biliary epithelial cells (64). Diffusion (accumulation) of free bile acids may trigger ductular reaction (hyperplastic response of bile duct epithelial cells), resulting in activation of cholangiocytes and portal fibroblasts. The mechanism of PF activation is poorly understood. Here, we propose that TCA bile acid can directly activate PFs (but not HSCs) into myofibroblasts, and this effect may rely on TCA-induced induced cytotoxicity, because PFs have been reported to lack the bile acid receptors FXR (farnesoid X receptor) and TGR5 (the membrane G protein-coupled

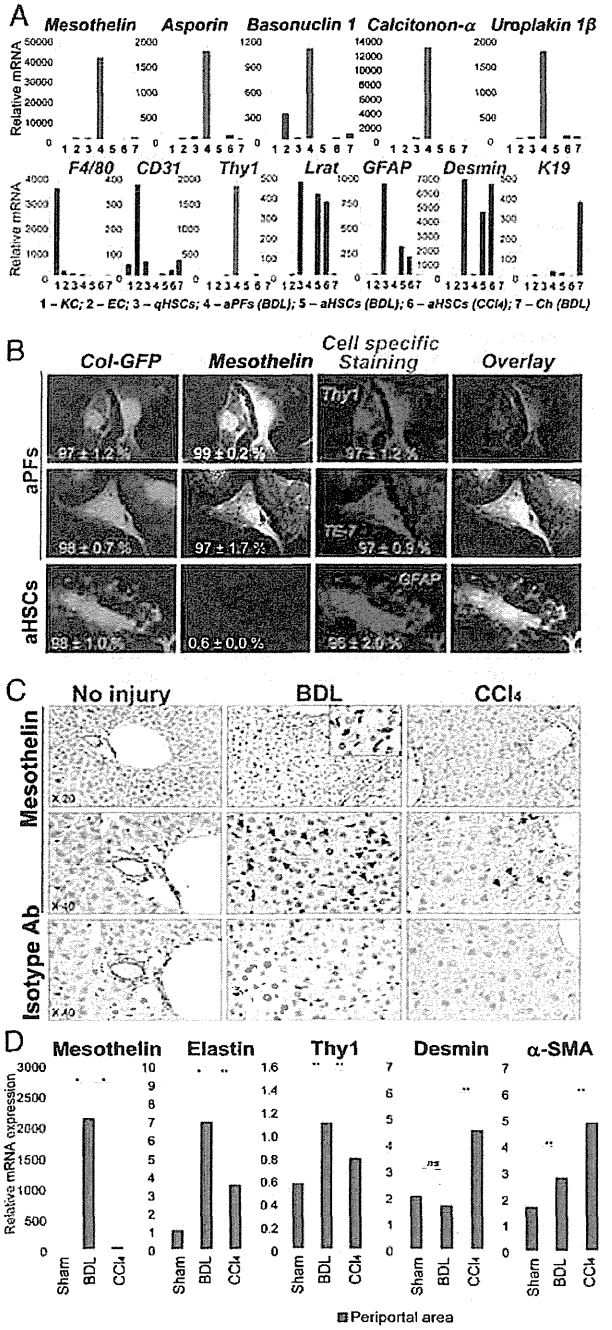

Fig. 5. Expression of mesothelin in aPFs is associated with cholestatic liver fibrosis in mice. (*A*) Expression of selected signature genes was compared by RT-PCR in aPFs and other cells in the liver. *Mesothelin, asporin, basonuclin 1, calcitonin-α,* and *uroplakin 1β* mRNA were up-regulated in BDL- (17 d) aPFs, but not in KC, endothelial cells (EC), BDL- and CCl_4-aHSCs and qHSCs, or BDL-induced cholangiocytes (Ch). The purity of each fraction was estimated by expression of F4/80 in KC, CD31 in EC, Lrat, GFAP, and Desmin in HSCs, Thy1 in aPFs, and K19 in cholangiocytes. The data (from three independent experiments) are shown as relative mRNA expression, $P < 0.01$. (*B*) aPFs and aHSCs were isolated from BDL (17 d)-injured Col-GFP mice and stained with anti-mesothelin Ab. Expression of Mesothelin was detected only in aPFs (but not in $GFAP^+$ aHSCs) and colocalized with Elastin (TE-7) and Thy1 staining. The percent of immunostained cells is calculated, $P < 0.05$ (four independent experiments; Fig. S7*B*). (*C*) Paraffin sections of liver tissue from BDL- (17 d) or CCl_4- (1.5 mo)treated mice ($n = 4$ per group) were immunostained with anti-mesothelin antibody or isotype-matched control. Expression of mesothelin was detected in BDL mice but not in sham-operated mice. Only a few mesothelin positive cells were detected in CCl_4-treated mice. Representative images are shown using 20× and 40× objective, (Fig. S7*C*). (*D*) Up-regulation of mesothelin is detected by laser capture microdissection in BDL-induced (but not CCl_4-induced) liver fibrosis. Laser capture microdissection was used to isolate periportal myofibroblasts from BDL (20 d) mice and CCl_4 (1.5 mo)-treated mice ($n = 3$ per group), cells were analyzed by RT-PCR for expression of aPF- and aHSC-specific markers. Mesothelin, elastin, and Thy1 were highly expressed in myofibroblasts obtained from periportal area of BDL liver. Desmin was expressed at high levels in CCl_4-treated liver. Unlike desmin, mesothelin was not expressed in CCl_4-treated periportal area. The data (from three independent experiments) are mRNA fold induction compared with periportal area of sham mice, $^*P < 0.01$; $^{**}P < 0.05$; ns, non-significant.

receptor) (65, 66). TCA-induced activation of PFs appears to be specific, and stimulation with other bile acids (TUDCA, DCA, TCDCA, TbMCA, CA) did not induce fibrogenic gene expression in PFs. However, unresponsiveness of PFs to tested bile acids may result from already high activation of isolated PFs (5 d after BDL), the lack of corresponding receptors (65), or poor experimental conditions (67). In addition, individual bile acids may produce other effects on PFs, such as cellular proliferation and cytokine secretion (17), which were not evaluated in this study. Furthermore, our in vitro conditions may not mimic the complex liver microenvironment required for bile acid stimulation of PFs (17). Alternatively, bile acids may indirectly induce PF activation by affecting cholangiocytes (68) or hepatocytes (65) that, in turn, may facilitate selective aPF activation via cell-cell signaling or cytokine secretion (64). In addition, specific factors produced by activated cholangiocytes may presensitize PFs for bile acid stimulation (69).

aPFS May Facilitate Activation of HSCs in BDL Model of Liver Injury. Another characteristic feature of aPFs is expression of IL-25R. Up-regulation of proinflammatory IL-17A, IL-25, IL-22, and IL-6 in the serum and in the liver accompany development of BDL-induced liver fibrosis (28). Therefore, it is not surprising that IL-25 may stimulate aPFs. Similar to other cell types, IL-25 induced secretion of IL-13 by aPFs, but did not further their activation. IL-13 has been implicated in pathogenesis of *Schistosoma mansoni* infection-induced liver fibrosis (70), and recently IL-13 was shown to directly stimulate HSCs to produce CTGF and subsequently upegulate fibrogenic genes in response to nonparasite liver injury (71). Therefore, we hypothesized that following BDL, IL-25–stimulated aPFs secrete IL-13, which facilitates HSC activation (via induction of *IL-13Ra2, Col1a1, Eotaxin, Tenascin-C, fibronection*, and phosphorylation of ERK1/2). Supporting this notion, bone marrow transplantation in $Abcb4^{-/-}$ mice lessened hepatic fibrosis via Th1 responses, but did not alter the level of IL-13 production (72), suggesting there must be an endogenous source of IL-13 in these mice. Further studies are required to determine the mechanism of HSC activation in response to cholestatic liver injury.

Proposed Novel Markers of Portal Fibroblasts. Robust markers of aHSCs and aPFs are needed. Our data confirmed that expression of Thy1 and Elastin distinguishes $Vit.A^-GFAP^-Desmin^-CD146^-$ aPFs from $Vit.A^+GFAP^+Desmin^+CD146^+Thy1^-Elastin^-$ aHSCs. Using gene expression profiling of in vivo aHSCs and aPFs, we have identified that mesothelin, calcitonin α, uroplakin 1β, basonclin 1, asporin, IL-18R1, and IL-25R may serve as additional useful markers to distinguish aPFs from aHSCs and myofibroblasts of other origins. We determined that these genes are highly expressed in portal fibroblasts but not in other cell types in fibrotic liver.

Interestingly, aPFs express mesothelin, calcitonin α, uroplakin 1β, basonclin 1, asporin, and IL-18R1 genes. The hepatic mesothelium is the source of HSCs and PFs during development (51, 60). Previous studies have demonstrated that the genes mentioned above and other genes [e.g., glycoprotein m6a, mesothelin, Uroplakin 1β and 3 β, Cyp2s1, mucin 16, crystalline, Prss12, Slipi, Caveolin, Dermokin, Calcitonin-related peptide, vanin, cytokeratin 7, Slc9a3r1, and Slc39a8 (metal ion transporter)], Igfbp6, see Fig. S6) are expressed in hepatic mesothelium (48). Furthermore, the gene expression profiles of epicardium isolated from adult mouse infarction-injured hearts identified the same genes among epicardium-specific signature genes, and for the first time, to our knowledge, implicated these genes (alone or in combination) in wound healing (49). Morphological studies have suggested that septum transversum mesenchyme (STM) is the source of hepatic mesenchymal cells (HSCs and perivascular mesenchymal cells) (73) and cardiac mesoderm [that gives rise to epicardium (74)]. Therefore, a common origin of hepatic mesothelium and epicardium may explain the similarity of gene expression profile of these tissues. During development, hepatic mesothelium undergoes an epithelial-to-mesenchymal (EMT) transition to produce PFs and HSCs. Furthermore, the expression of WT1, a mesothelial-specific factor (60), is expressed in aPFs (vs. aHSCs; Fig. S6). Because both hepatic mesothelium and epicardium can contribute to myofibroblasts in their respective organs, the contribution of the aforementioned genes to repair and fibrosis should be addressed.

Mesothelin is a glycosyl phosphatidylinositol (GPI)-anchored membrane glycoprotein that is expressed in normal mesothelial cells. It is also highly expressed in several species of malignant tumors, such as mesothelioma as well as ovarian and pancreatic cancers (75–77). We determined that mesothelin (Msln)-deficient mice are less susceptible to liver fibrosis compared with the wild-type mice. Previous studies have implicated mesothelin in mediation of cellular interaction and metastatic dissemination. Because of a strong induction in different types of cancer, mesothelin is considered as a tumor-associated antigen, which serves as a prognostic marker of disease progression, and became a therapeutic target for anti-cancer therapy. Here we demonstrate that mesothelin is highly expressed in aPFs in response to BDL, so that mesothelin may serve as a novel marker of aPFs and a potential target for antifibrotic therapy.

Materials and Methods

Mice and Liver Injury. Collagen α1(I)-GFP mice (22) and wild-type littermates were used at 8 wk of age, in C57BL/6 background. Liver injury was induced in mice by CCl_4 (1:4 dilution in corn oil, 60 μL × 14 injections; ref. 41) or ligation of the common bile duct (20 d) (41). Mice were maintained under specific pathogen free conditions at the animal facilities of University of California, San Diego (protocol S07088 approved by Institutional Animal Care and Use Committee).

Isolation of Nonparenchymal Fraction. Livers were perfused and digested by using the pronase/collagenase method (41), and cells were centrifuged to pellet the hepatocytes. The remaining nonparenchymal cell fraction [containing hepatic myofibroblasts (HSCs, portal fibroblasts, and others), Kupffer cells, BM cells, and endothelial cells] (41). aPFs and aHSCs were isolated by using cell sorting for Col-GFP$^+$Vit.A$^-$ and Col-GFP$^+$Viat.A$^+$ cells. Kupffer cells (KC) and endothelial cells were isolated by gradient centrifugation (15% Nycodenz) following by magnetic sorting with anti-CD11b and anti-CD31 antibodies, respectively (Miltenyi Biotec). Cholangiocytes were a gift of *Gianfranco Alpini* (Texas A&M Health Science Center, Central Texas Veterans Health Care System, Temple, TX) and were isolated from BDL mice (78).

Flow cytometry. Flow cytometry was based on simultaneous detection of collagen-α1(I)-GFP (488 nm) and vitamin A (autofluorescent signal detected by violet laser at 405 nm; Fig. 2*B*) in Col-GFP mice (40). Phenotyping of the nonparenchymal fraction isolated from Col-GFP mouse livers ($n = 6$ time point) was performed on Canto (BD). Cell sorting was performed on a MoFlo (Beckman Coulter).

Immunofluorescence and immunohistochemistry. Formalin-fixed frozen livers were stained with Sirius Red and anti–α-SMA Ab (Abcam). Immunohistochemistry was performed by using DAB staining (Vector) and counterstaining with Hematoxilin. Immunocytochemistry is described in *SI Materials and Methods*.

Whole Mouse Genome Gene Expression Microarray. The gene expression profile of qHSCs, CCl_4- (1.5 mo) aHSCs, BDL- (20 d) aHSCs, and PFs was studied by using Whole Mouse Genome Microarray (Agilent) (40). See *SI Materials and Methods* for details.

Characterization of IL-13 Signaling in Human HSCs. Human stellate cells (ScienCell) were plated overnight, then serum-starved for 6 h and stimulated with IL-13, TGFβ1 (R&D Systems), or a combination of both. CCL11/eotaxin was measured in cell-free supernatants 48 h after stimulation with IL-13 by sandwich ELISA (RnD Systems). Gene expression was assessed at 24 h by quantitative RT-PCR.

Quantitative RT-PCR. Total RNA was isolated from the nonparenchymal fraction, hepatocyte fraction, or purified Col$^+$Vit.A$^+$ and Col$^+$Vit.A$^+$ cells or hepatic stellate cells by using RNeasy columns (Qiagen). Gene expression levels were calculated after normalization to the standard housekeeping gene 18S by using the ΔΔ CT method as described by the manufacturer (Invitrogen) and expressed as relative mRNA levels compared with control. The results are represented as mean ± SEM, $P < 0.0001$.

Laser Capture Microdissection and RNA Extraction. Livers from sham-, CCl_4- and BDL-injured mice were snap-frozen in FSC 22 Frozen Section Media (Leica Microsystems) and stored at −80 °C. Transverse sections (10 μm) were cut with a cryostat at −20 °C. Cryosections were mounted on membrane-coated slides. A Leica LMD7000 system (Leica Microsystems) was used to cut periportal or centrilobular area on sections. Microdissected sections were collected in the lid of a 0.5-mL microtube containing RLT buffer from the RNeasy (Qiagen). Total RNA was extracted by using the same kit and following the manufacturer's instructions.

ACKNOWLEDGMENTS. We thank Dr. Sato and Dr. Uehiro for initial technical assistance with laser capture microdissection and Tom Kisby and Rebecca Dunmore for technical assistance with the in vitro studies using human HSCs. This work was supported by National Institutes of Health Grants DK088837, GM41804, AA15055, DK72237, AI0777802, and P50 AA011999; the Japanese Ministry of Health, Labour, and Welfare; and the American Liver Foundation.

1. Bataller R, Brenner DA (2005) Liver fibrosis. *J Clin Invest* 115(2):209–218.
2. Forbes SJ, Parola M (2011) Liver fibrogenic cells. *Best Pract Res Clin Gastroenterol* 25(2):207–217.
3. Kisseleva T, et al. (2006) Bone marrow-derived fibrocytes participate in pathogenesis of liver fibrosis. *J Hepatol* 45(3):429–438.
4. Kisseleva T, et al. (2011) Fibrocyte-like cells recruited to the spleen support innate and adaptive immune responses to acute injury or infection. *J Mol Med (Berl)* 89(10):997–1013.
5. Scholten D, et al. (2011) Migration of fibrocytes in fibrogenic liver injury. *Am J Pathol* 179(1):189–198.
6. Kalluri R (2009) EMT: When epithelial cells decide to become mesenchymal-like cells. *J Clin Invest* 119(6):1417–1419.
7. Choi SS, Diehl AM (2009) Epithelial-to-mesenchymal transitions in the liver. *Hepatology* 50(6):2007–2013.
8. Taura K, et al. (2010) Hepatocytes do not undergo epithelial-mesenchymal transition in liver fibrosis in mice. *Hepatology* 51(3):1027–1036.
9. Scholten D, et al. (2010) Genetic labeling does not detect epithelial-to-mesenchymal transition of cholangiocytes in liver fibrosis in mice. *Gastroenterology* 139(3):987–998.
10. Chu AS, et al. (2011) Lineage tracing demonstrates no evidence of cholangiocyte epithelial-to-mesenchymal transition in murine models of hepatic fibrosis. *Hepatology* 53(5):1685–1695.
11. Dranoff JA, Wells RG (2010) Portal fibroblasts: Underappreciated mediators of biliary fibrosis. *Hepatology* 51(4):1438–1444.
12. Bhunchet E, Wake K (1992) Role of mesenchymal cell populations in porcine serum-induced rat liver fibrosis. *Hepatology* 16(6):1452–1473.
13. Desmoulière A, et al. (1997) Extracellular matrix deposition, lysyl oxidase expression, and myofibroblastic differentiation during the initial stages of cholestatic fibrosis in the rat. *Lab Invest* 76(6):765–778.
14. Uchio K, et al. (2002) Cellular retinol-binding protein-1 expression and modulation during in vivo and in vitro myofibroblastic differentiation of rat hepatic stellate cells and portal fibroblasts. *Lab Invest* 82(5):619–628.
15. Wen JW, Olsen AL, Perepelyuk M, Wells RG (2012) Isolation of rat portal fibroblasts by in situ liver perfusion. *J Vis Exp* (64):3669.
16. Kruglov EA, Jain D, Dranoff JA (2002) Isolation of primary rat liver fibroblasts. *J Investig Med* 50(3):179–184.

17. Clouzeau-Girard H, et al. (2006) Effects of bile acids on biliary epithelial cell proliferation and portal fibroblast activation using rat liver slices. *Lab Invest* 86(3): 275–285.
18. Knittel T, et al. (1999) Rat liver myofibroblasts and hepatic stellate cells: Different cell populations of the fibroblast lineage with fibrogenic potential. *Gastroenterology* 117(5):1205–1221.
19. Goodpaster T, et al. (2008) An immunohistochemical method for identifying fibroblasts in formalin-fixed, paraffin-embedded tissue. *J Histochem Cytochem* 56(4): 347–358.
20. Dranoff JA, et al. (2002) The ecto-nucleoside triphosphate diphosphohydrolase NTPDase2/CD39L1 is expressed in a novel functional compartment within the liver. *Hepatology* 36(5):1135–1144.
21. Bosselut N, et al. (2010) Distinct proteomic features of two fibrogenic liver cell populations: Hepatic stellate cells and portal myofibroblasts. *Proteomics* 10(5):1017–1028.
22. Yata Y, et al. (2003) DNase I-hypersensitive sites enhance alpha1(I) collagen gene expression in hepatic stellate cells. *Hepatology* 37(2):267–276.
23. Brenner DA, Rippe RA, Veloz L (1989) Analysis of the collagen alpha 1(I) promoter. *Nucleic Acids Res* 17(15):6055–6064.
24. Österreicher CH, et al. (2010) Fibroblast specific protein 1 identifies a subpopulation of liver inflammatory macrophages. *Proc Natl Acad Sci USA* 108(1):308–13.
25. De Minicis S, et al. (2007) Gene expression profiles during hepatic stellate cell activation in culture and in vivo. *Gastroenterology* 132(5):1937–1946.
26. Inokuchi S, et al. (2011) Toll-like receptor 4 mediates alcohol-induced steatohepatitis through bone marrow-derived and endogenous liver cells in mice. *Alcohol Clin Exp Res* 35(8):1509–1518.
27. Lin SL, Kisseleva T, Brenner DA, Duffield JS (2008) Pericytes and perivascular fibroblasts are the primary source of collagen-producing cells in obstructive fibrosis of the kidney. *Am J Pathol* 173(6):1617–1627.
28. Meng F, et al. (2012) Interleukin-17 signaling in inflammatory, Kupffer cells, and hepatic stellate cells exacerbates liver fibrosis in mice. *Gastroenterology* 143(3): 765–776, e761-763.
29. Meurer SK, et al. (2013) Overexpression of endoglin modulates TGF-β1-signalling pathways in a novel immortalized mouse hepatic stellate cell line. *PLoS ONE* 8(2): e56116.
30. Parsons CJ, et al. (2011) Mutation of the 5′-untranslated region stem-loop structure inhibits α1(I) collagen expression in vivo. *J Biol Chem* 286(10):8609–8619.
31. Stefanovic B, Brenner DA (2003) 5′ stem-loop of collagen alpha 1(I) mRNA inhibits translation in vitro but is required for triple helical collagen synthesis in vivo. *J Biol Chem* 278(2):927–933.
32. Stefanovic B, et al. (1997) Posttranscriptional regulation of collagen alpha1(I) mRNA in hepatic stellate cells. *Mol Cell Biol* 17(9):5201–5209.
33. Stefanovic B, Lindquist J, Brenner DA (2000) The 5′ stem-loop regulates expression of collagen alpha1(I) mRNA in mouse fibroblasts cultured in a three-dimensional matrix. *Nucleic Acids Res* 28(2):641–647.
34. Stefanovic B, Schnabl B, Brenner DA (2002) Inhibition of collagen alpha 1(I) expression by the 5′ stem-loop as a molecular decoy. *J Biol Chem* 277(20):18229–18237.
35. Stefanovic L, Brenner DA, Stefanovic B (2005) Direct hepatotoxic effect of KC chemokine in the liver without infiltration of neutrophils. *Exp Biol Med (Maywood)* 230(8):573–586.
36. Taura K, et al. (2008) Hepatic stellate cells secrete angiopoietin 1 that induces angiogenesis in liver fibrosis. *Gastroenterology* 135(5):1729–1738.
37. Magness ST, Bataller R, Yang L, Brenner DA (2004) A dual reporter gene transgenic mouse demonstrates heterogeneity in hepatic fibrogenic cell populations. *Hepatology* 40(5):1151–1159.
38. Magness ST, Brenner DA (1999) Targeted disruption of the mouse ferrochelatase gene producing an exon 10 deletion. *Biochim Biophys Acta* 1453(1):161–174.
39. Bataller R, et al. (2003) NADPH oxidase signal transduces angiotensin II in hepatic stellate cells and is critical in hepatic fibrosis. *J Clin Invest* 112(9):1383–1394.
40. Kisseleva T, et al. (2012) Myofibroblasts revert to an inactive phenotype during regression of liver fibrosis. *Proc Natl Acad Sci USA* 109(24):9448–9453.
41. Seki E, et al. (2007) TLR4 enhances TGF-beta signaling and hepatic fibrosis. *Nat Med* 13(11):1324–1332.
42. Perepelyuk M, et al. (2013) Hepatic stellate cells and portal fibroblasts are the major cellular sources of collagens and lysyl oxidases in normal liver and early after injury. *Am J Physiol Gastrointest Liver Physiol* 304(6):G605–G614.
43. Fort MM, et al. (2001) IL-25 induces IL-4, IL-5, and IL-13 and Th2-associated pathologies in vivo. *Immunity* 15(6):985–995.
44. Gregory LG, et al. (2012) 25 drives remodelling in allergic airways disease induced by house dust mite. *Thorax* 68(1):82–90.
45. Liu Y, et al. (2011) IL-13 induces connective tissue growth factor in rat hepatic stellate cells via TGF-β-independent Smad signaling. *J Immunol* 187(5):2814–2823.
46. Pope SM, et al. (2005) Identification of a cooperative mechanism involving interleukin-13 and eotaxin-2 in experimental allergic lung inflammation. *J Biol Chem* 280(14):13952–13961.
47. Jinnin M, et al. (2006) Upregulation of tenascin-C expression by IL-13 in human dermal fibroblasts via the phosphoinositide 3-kinase/Akt and the protein kinase C signaling pathways. *J Invest Dermatol* 126(3):551–560.
48. Onitsuka I, Tanaka M, Miyajima A (2010) Characterization and functional analyses of hepatic mesothelial cells in mouse liver development. *Gastroenterology* 138(4): 1525–1535, e1521–1526.
49. Bochmann L, et al. (2010) Revealing new mouse epicardial cell markers through transcriptomics. *PLoS ONE* 5(6):e11429.
50. Asahina K (2012) Hepatic stellate cell progenitor cells. *J Gastroenterol Hepatol* 27 (Suppl 2):80–84.
51. Asahina K, et al. (2009) Mesenchymal origin of hepatic stellate cells, submesothelial cells, and perivascular mesenchymal cells during mouse liver development. *Hepatology* 49(3):998–1011.
52. Glaser SS, et al. (2007) Knockout of alpha-calcitonin gene-related peptide reduces cholangiocyte proliferation in bile duct ligated mice. *Lab Invest* 87(9):914–926.
53. Chang K, Pastan I (1996) Molecular cloning of mesothelin, a differentiation antigen present on mesothelium, mesotheliomas, and ovarian cancers. *Proc Natl Acad Sci USA* 93(1):136–140.
54. Grigoriu BD, Grigoriu C, Chahine B, Gey T, Scherpereel A (2009) Clinical utility of diagnostic markers for malignant pleural mesothelioma. *Monaldi Arch Chest Dis* 71(1): 31–38.
55. Bera TK, Pastan I (2000) Mesothelin is not required for normal mouse development or reproduction. *Mol Cell Biol* 20(8):2902–2906.
56. Lujambio A, et al. (2013) Non-cell-autonomous tumor suppression by p53. *Cell* 153(2): 449–460.
57. Krizhanovsky V, et al. (2008) Senescence of activated stellate cells limits liver fibrosis. *Cell* 134(4):657–667.
58. Henderson NC, et al. (2013) Targeting of αv integrin identifies a core molecular pathway that regulates fibrosis in several organs. *Nat Med* 19(12):1617–1624.
59. Mederacke I, et al. (2013) Fate tracing reveals hepatic stellate cells as dominant contributors to liver fibrosis independent of its aetiology. *Nat Commun* 4:2823.
60. Asahina K, Zhou B, Pu WT, Tsukamoto H (2011) Septum transversum-derived mesothelium gives rise to hepatic stellate cells and perivascular mesenchymal cells in developing mouse liver. *Hepatology* 53(3):983–995.
61. Desmoulière A (2007) Hepatic stellate cells: The only cells involved in liver fibrogenesis? A dogma challenged. *Gastroenterology* 132(5):2059–2062.
62. Tang L, Tanaka Y, Marumo F, Sato C (1994) Phenotypic change in portal fibroblasts in biliary fibrosis. *Liver* 14(2):76–82.
63. Tuchweber B, Desmoulière A, Bochaton-Piallat ML, Rubbia-Brandt L, Gabbiani G (1996) Proliferation and phenotypic modulation of portal fibroblasts in the early stages of cholestatic fibrosis in the rat. *Lab Invest* 74(1):265–278.
64. Syal G, Fausther M, Dranoff JA (2012) Advances in cholangiocyte immunobiology. *Am J Physiol Gastrointest Liver Physiol* 303(10):G1077–G1086.
65. Fickert P, et al. (2009) Farnesoid X receptor critically determines the fibrotic response in mice but is expressed to a low extent in human hepatic stellate cells and periductal myofibroblasts. *Am J Pathol* 175(6):2392–2405.
66. Fausther M, Dranoff JA (2011) New insights on the pathogenesis of biliary cirrhosis provided by studies in FXR knockout mice. *J Hepatol* 55(4):939–940.
67. Guyot C, et al. (2010) Fibrogenic cell phenotype modifications during remodelling of normal and pathological human liver in cultured slices. *Liver Int* 30(10):1529–1540.
68. Keitel V, et al. (2009) The membrane-bound bile acid receptor TGR5 is localized in the epithelium of human gallbladders. *Hepatology* 50(3):861–870.
69. Fabris L, Strazzabosco M (2011) Epithelial-mesenchymal interactions in biliary diseases. *Semin Liver Dis* 31(1):11–32.
70. Wynn TA (2003) IL-13 effector functions. *Annu Rev Immunol* 21:425–456.
71. Liu Y, Munker S, Müllenbach R, Weng HL (2012) IL-13 signaling in liver fibrogenesis. *Front Immunol* 3:116.
72. Roderfeld M, et al. (2012) Bone marrow transplantation improves hepatic fibrosis in Abcb4-/- mice via Th1 response and matrix metalloproteinase activity. *Gut* 61(6): 907–916.
73. Enzan H, et al. (1997) Development of hepatic sinusoidal structure with special reference to the Ito cells. *Microsc Res Tech* 39(4):336–349.
74. Zhou B, et al. (2008) Epicardial progenitors contribute to the cardiomyocyte lineage in the developing heart. *Nature* 454(7200):109–113.
75. Hassan R, Bera T, Pastan I (2004) Mesothelin: A new target for immunotherapy. *Clin Cancer Res* 10(12 Pt 1):3937–3942.
76. Scholler N, et al. (1999) Soluble member(s) of the mesothelin/megakaryocyte potentiating factor family are detectable in sera from patients with ovarian carcinoma. *Proc Natl Acad Sci USA* 96(20):11531–11536.
77. Sapede C, et al. (2008) Aberrant splicing and protease involvement in mesothelin release from epithelioid mesothelioma cells. *Cancer Sci* 99(3):590–594.
78. Woo K, et al. (2010) Adenosine triphosphate release and purinergic (P2) receptor-mediated secretion in small and large mouse cholangiocytes. *Hepatology* 52(5): 1819–1828.

Nutrition 30 (2014) 1195–1207

Contents lists available at ScienceDirect

Nutrition

journal homepage: www.nutritionjrnl.com

Basic nutritional investigation

Whey-hydrolyzed peptide-enriched immunomodulating diet prevents progression of liver cirrhosis in rats

Kanta Jobara M.D. [a], Toshimi Kaido M.D., Ph.D. [a,*], Tomohide Hori M.D., Ph.D. [a], Keiko Iwaisako M.D., Ph.D. [b], Kosuke Endo M.D. [a], Yoichiro Uchida M.D., Ph.D. [a], Shinji Uemoto M.D., Ph.D. [a]

[a] *Division of Hepato-Biliary-Pancreatic and Transplant Surgery, Department of Surgery, Kyoto University Graduate School of Medicine, Kyoto, Japan*

[b] *Department of Target Therapy Oncology, Kyoto University Graduate School of Medicine, Kyoto, Japan*

ARTICLE INFO

Article history:
Received 14 September 2013
Accepted 5 February 2014

Keywords:
Whey-hydrolyzed peptide
Immunomodulating diet
Liver fibrosis
Cirrhosis
Antifibrotic
Hepatocytes-protective

ABSTRACT

Objective: Liver fibrosis and subsequent cirrhosis is a major cause of death worldwide, but few effective antifibrotic therapies are reported. Whey-hydrolyzed peptide (WHP), a major peptide component of bovine milk, exerts anti-inflammatory effects in experimental models. A WHP-enriched diet is widely used for immunomodulating diets (IMD) in clinical fields. However, the effects of WHP on liver fibrosis remain unknown. The aim of this study was to investigate the antifibrotic effects of WHP in a rat cirrhosis model.

Methods: Progressive liver fibrosis was induced by repeated intraperitoneal administration of dimethylnitrosamine (DMN) for 3 wk. Rats were fed either a WHP-enriched IMD (WHP group) or a control enteral diet (control group). The degree of liver fibrosis was compared between groups. Hepatocyte-protective effects were examined using hepatocytes isolated from rats fed a WHP diet. Reactive oxygen species and glutathione in liver tissue were investigated in the DMN cirrhosis model.

Results: Macroscopic and microscopic progression of liver fibrosis was remarkably suppressed in the WHP group. Elevated serum levels of liver enzymes and hyaluronic acid, and liver tissue hydroxyproline content were significantly attenuated in the WHP group. Necrotic hepatocyte rates with DMN challenge, isolated from rats fed a WHP-enriched IMD, were significantly lower. In the DMN cirrhosis model, reactive oxygen species were significantly lower, and glutathione was significantly higher in the WHP group's whole liver tissue.

Conclusion: A WHP-enriched IMD effectively prevented progression of DMN-induced liver fibrosis in rats via a direct hepatocyte-protective effect and an antioxidant effect through glutathione synthesis.

Introduction

Liver cirrhosis is the end stage of chronic liver injury resulting from various causes, such as viral or alcoholic hepatitis, and non-alcoholic steatohepatitis [1]. It is histopathologically characterized as the loss of hepatocytes with interstitial fibrosis [2]. Progression of fibrosis and subsequent cirrhosis lead to life-threatening liver failure and carcinogenesis [1,3]. Despite extensive research on liver cirrhosis, there are few medications (without adverse side effects) proven to be clinically useful for prevention or slowing the progression of liver fibrosis [4,5]. Therefore, new antifibrotic agents with less toxicity are needed for the management and prevention of liver fibrosis [6].

Continuous hepatocellular damage caused by virus and alcohol introduces an inflammatory response with release of inflammatory cytokines, such as interleukin (IL)-6, tumor necrosis factor (TNF)-α, and IL-10. These inflammatory cytokines promote remodeling and macrophage phagocytosis of necrotic hepatocytes. Subsequent activation of hepatic stellate cells (HSCs) by transforming growth factor (TGF)-β promotes

KJ, TK, and KI designed the research. TK, TH, and SU conducted the research. KJ, TK, TH, KI, KE, and YU analyzed the data. KJ wrote the initial draft. KJ, TK, TH, and KI reworked further drafts, and TK and SU had primary responsibility for the final content. All authors read and approved the final manuscript.

* Corresponding author. Tel.: +81 75 751 4322; fax: +81 75 751 4348.
E-mail address: Kaido@kuhp.kyoto-u.ac.jp (T. Kaido).

0899-9007/$ - see front matter © 2014 Elsevier Inc. All rights reserved.
http://dx.doi.org/10.1016/j.nut.2014.02.005

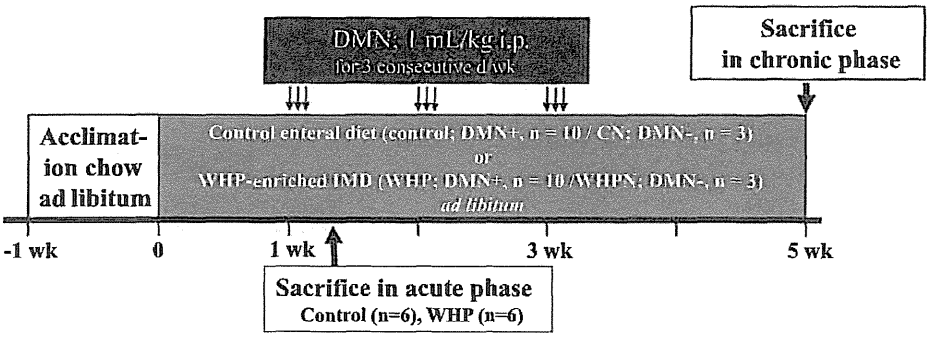

Fig. 1. Experimental protocols in vivo. CN, control diet without DMN as negative control for DMN; DMN, dimethylnitrosamine; IMD, immunomodulating diet; WHP, whey-hydrolyzed peptide; WHPN, whey-hydrolyzed peptide diet without DMN as negative control for DMN.

production extracellular matrix and leads to liver fibrosis [7,8]. Reactive oxygen species (ROS) are involved in liver injury, and antioxidants may protect hepatocytes and prevent following liver fibrosis [9]. Moreover, hepatocellular damages and inflammatory cytokines interact with each other.

Recent nutritional studies demonstrated that bovine milk proteins have many effects for health benefits, such as preventing weight gain and enhancing bone architecture [10]. Whey-hydrolyzed peptide (WHP) is a major peptide component of bovine milk. A WHP-enriched diet is one form of immunomodulating diet (IMD) that has been widely used for nutritional support in patients with malnutrition or insufficient oral intake. A WHP-enriched IMD exerts antioxidant, anti-inflammatory, immunomodulating, and antibacterial effects in some experimental models [11–15]. The clinical utility of this novel WHP-enriched IMD has been documented, mainly at the perioperative period [16–18]. Previous research has indicated that a WHP-enriched diet exerts an anti-inflammatory effect, and may have therapeutic potential [11].

The present study investigated the antifibrotic effects of WHP in a rat liver cirrhosis model with progressive fibrosis. We also discuss the therapeutic potential of WHP against progressive fibrosis and possible mechanisms during liver cirrhosis progression from a literature review.

Materials and methods

Rats

Male Sprague-Dawley rats (6 wk old) were purchased from Japan SLC, Inc. (Hamamatsu, Japan). Rats were cared for according to the Institutional Guidelines for Animal Welfare. All experimental procedures were approved by the Institutional Animal Care and Use Committee of Kyoto University (Protocol ID: MedKyo12521).

Immunomodulating diet

Rats were fed conventional chow as a control enteral diet (MEIBALANCE; Meiji Dairies Co., Tokyo, Japan) or a WHP-enriched IMD (MEIN; Meiji Dairies Co.) ad libitum throughout the experiments (Fig. 1). The compositions of the two diets were almost identical, except for the protein source as summarized in Table 1 (casein in the control diet, and WHP in the WHP-enriched IMD).

Liver cirrhosis model rats

One week after starting diets, rats were intraperitoneally given dimethylnitrosamine (DMN; 1% dissolved in saline; 1 mL/kg; Tokyo Chemical Industry Co. Ltd., Tokyo, Japan) consecutively for 3 d each week for 3 wk to induce progressive fibrosis and subsequent cirrhosis [19,20] (Fig. 1).

Histopathologic assessment

Liver specimens were fixed in 4% paraformaldehyde, embedded in paraffin, serially cut into thin slices (3 μm thick). Slides were stained with hematoxylin

Table 1
Diet composition*

	Control	WHP-enriched IMD
Proteins (g)	5.0	5.0
Protein (% kcal)	20.0	20.0
Protein sources	Total milk protein Na caseinate	Whey peptides Fermented milk
Carbohydrates (g)	15.3	14.5
Carbohydrates (% kcal)	57.5	55
CHO sources	Dextrin	Isomaltulose Dextrin
Lipids (g)	2.50	2.80
Lipids (% kcal)	22.5	25.0
MCT (g)	-	0.59
EPA, DHA (g)	-	0.060
ω-6/ω-3	3.2	2.0
Vitamins		
Vitamin A (g RE)	60.0	150
Vitamin D (g)	0.50	0.75
Vitamin E (mg)	3.0	5.0
Vitamin K (g)	5.0	3.4
Vitamin B1 (mg)	0.15	0.25
Vitamin B2 (mg)	0.20	0.30
Niacin (mg)	1.6	3.0
Vitamin B6 (mg)	0.30	0.30
Vitamin B12 (g)	0.60	0.60
Folic acid (g)	50	50
Biotin (g)	15	7.5
Pantothenic acid	0.60	1.2
Vitamin C (mg)	16	50
Choline (mg)	1.8	9.2
Carnitine (mg)	-	15
Minerals		
Sodium (mg)	110	70
Potassium (mg)	100	80
Calcium (mg)	70	80
Magnesium (mg)	30	20
Phosphorus (mg)	70	70
Iron (mg)	1.0	1.0
Zinc (mg)	1.0	1.0
Copper (mg)	0.050	0.050
Manganese (mg)	0.230	0.175
Chromium (g)	3.00	2.96
Molybdenum (g)	2.5	2.5
Selenium (g)	6.0	5.0
Iodine (g)	15	9.7
Chloride (mg)	110	80

CHO, carbohydrate; DHA, docosahexaenoic acid; EPA, eicosapentaenoic acid; IMD, immunomodulating diet; RE, retinol equivalent; MCT, medium chain triglyceride; WHP, whey-hydrolyzed peptide; (-), no additives

* The major difference between WHP-enriched IMD and control enteral diet used in this study is the protein composition; the WHP-enriched IMD contains whey peptides and fermented milk product as the protein sources, whereas the control enteral diet contains total milk protein and sodium caseinate.

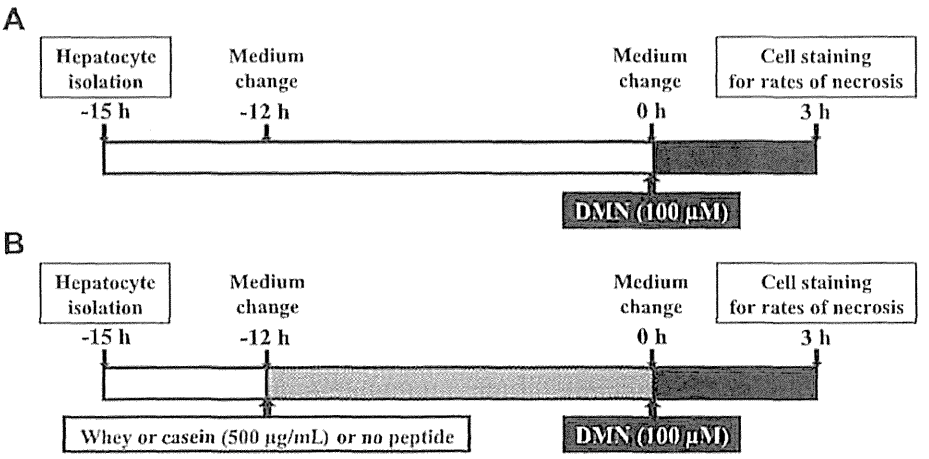

Fig. 2. Protocol for analysis of the hepatocyte-protective effect. (A) Protocol for analysis of the hepatocyte-protective effect in vivo for isolated hepatocytes from rats fed a WHP diet. (B) Protocol for analysis of the hepatocyte-protective effect in vitro for hepatocytes with WHP-added medium. DMN, dimethylnitrosamine; WHP, whey-hydrolyzed peptide.

and eosin and Mallory–Azan stain for histologic analysis of fibrosis. The degrees of liver fibrosis and histologic activity in native livers were scored according to the Metavir scoring system [21].

Immunohistochemistry

After blocking, sections were incubated with a primary antibody for α-smooth muscle actin (α-SMA) (ab5694; Abcam, Cambridge, UK) and then with a labeled polymer (Envision System/Horse radish peroxidase; Dako, Tokyo, Japan). Sections were examined after incubation with diamino benzidine (Liquid Diamino Benzidine Substrate Chromogen System; Dako). The α-SMA staining was analyzed using quantitative software (BZ-Analyzer; KEYENCE, Osaka, Japan), with detection thresholds set to the brown color (diamino benzidine color). Images of five non-overlapping fields were selected at random and captured per section at ×200 magnification. The degree of labeling in each section was determined from the area within the color range divided by the total area. For collagen I, we used primary antibody against collagen I (NB600-408; Novus Biologicals, Littleton, CO, USA) with biotinylated antibody-recognizing rabbit immunoglobulin G (BA-1000; Vector Laboratories, Burlingame, CA, USA). The positive areas of the staining were analyzed by quantitative software in the same way as α-SMA staining.

Hydroxyproline determination

For collagen quantification in the liver, hydroxyproline (the specific amino acid of type I collagen) was measured using the standard biochemical method described previously [22] Hydroxyproline was then quantitated photometrically at 558 nm from a standard curve generated using purified hydroxyproline (Sigma, Tokyo, Japan).

Hepatocyte isolation

Hepatocytes were isolated from rat livers as previously described [23,24]. Briefly, rat liver was perfused for 15 min with 0.03% collagenase (Wako, Kyoto, Japan). After collagenase perfusion, the cell suspension was centrifuged at 50g for 1 min.

Cell culture

Isolated hepatocytes were cultured on six-well plates coated with type I collagen at a cell density of 1×10^5 cells/well with serum-free Medium 199 Earle's liquid (Invitrogen, Tokyo, Japan), 100 U/mL penicillin, 100 μg/mL streptomycin, and 0.25 μg/mL of amphotericin B at 37°C.

Propidium iodide Hoechst ratio calculation for degree of hepatocyte necrosis

Cultured hepatocytes were stained with Hoechst 33342 (Nacalai Tesque, Kyoto, Japan) and propidium iodide (Calbiochem, San Diego, CA, USA) for DNA staining to evaluate cell viability. Double staining with propidium iodide (for dead cells) and Hoechst 33342 (for dead and viable cells) was used to differentiate necrotic cells from normal cells with a fluorescent microscope. Images of five non-overlapping fields at ×200 magnification were selected at random, and cells were automatically counted (BZ-II Analyzer; KEYENCE). The propidium iodide-positive ratio was calculated as the percentage of propidium iodide-positive cells among Hoechst 33342-positive cells [24].

Inflammatory cytokines in serum

Serum concentrations of IL-6, TNF-α, IL-10, and interferon (IFN)-γ were measured using conventional assay kits (Cytometric Bead Array Kits; Becton Dickinson Co., Franklin Lakes, NJ, USA).

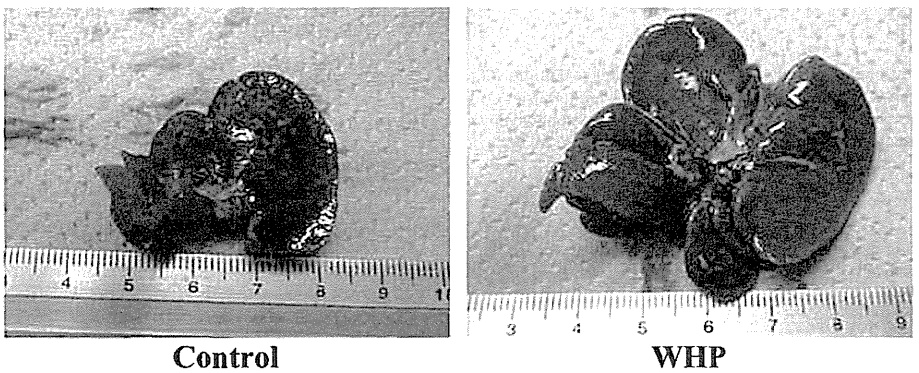

Fig. 3. Antifibrotic/cirrhotic effects of WHP in macroscopic findings of livers in the DMN-induced cirrhosis rat model (chronic phase). In the control group, a granular liver surface and remarkable atrophy were observed. Livers from the WHP group showed near normal findings and a non-damaged appearance. DMN, dimethylnitrosamine; WHP, whey-hydrolyzed peptide.

Table 2
Degree of cirrhosis (chronic phase)*

	Control (n = 10)	WHP (n = 10)	*P*-values
LC	6	0	0.003
Ascites	6	0	0.003
Body weight (g)	302 ± 27	307 ± 26	0.650
Liver weight (g)	6.8 ± 2.5	10.5 ± 1.9	0.007
Spleen weight (g)	1.7 ± 0.3	0.8 ± 0.2	<0.001

DMN, dimethylnitrosamine, LC, liver cirrhosis; WHP, whey-hydrolyzed peptide
* Macroscopic LC, ascites, liver atrophy, and splenomegaly were significantly suppressed in the WHP group in a DMN-induced cirrhosis rat model.

Quantitative reverse-transcription polymerase chain reaction analysis

Total RNA was extracted from liver samples using an assay kit (RNeasy Mini Kit with on-column DNA digestion; Qiagen, Tokyo, Japan). Total RNA was reverse transcribed to complementary DNA using an assay kit (Omniscript RT Kit; Qiagen, Valencia, CA, USA). Quantitative real-time reverse transcription polymerase chain reaction (RT-PCR) for IL-6 and TNF-α was performed (TaqMan Fast Universal PCR Master Mix; Applied Biosystems, Foster City, CA, USA) using a real-time quantitative thermal cycler (StepOnePlus; Applied Biosystems). Validated exon-spanning primers (TaqMan primers [B-actin Rn 00667869 _m1; IL-6 Rn 01410330_m1; TNF-α Rn 00562055 _m1]; Applied Biosystems) were used during amplification with B-actin as the internal control. PCR products were quantified using the 2-ΔΔCT method [25]. Quantitative RT-PCR for cytochrome P450 (CYP) 2 E1 was performed (SYBR Green Master reaction mix; Invitrogen, Carlsbad, CA, USA) using a real-time quantitative thermal cycler (StepOnePlus; Applied Biosystems). The relative abundance of the target genes was obtained by calculating against a standard curve and normalized to glyceraldehyde-3-phosphate dehydrogenase (GAPDH) as the internal control. Primer sequences used were as follow:

CYP2 E1-Forward: 5′-AGTCTGCCACCCTCTGCTTA-3′, CYP2 E1-Reverse: 5′-GAAAGCTGAGACCCATGAGC-3′, GAPDH-Forward: 5′-TGGAGTCTACTGGCGTCTT-3′, GAPDH-Reverse: 5′-TGTCATATTTCTCGTGGTTCA-3′.

Reactive oxygen species analysis for liver specimens in acute and chronic phases

Malondialdehyde (MDA) levels, a quantitative value of ROS, were determined according to the thiobarbituric acid method using a conventional assay kit (NWLSS MDA Assay Kit; Northwest Life Science Specialties, Vancouver, WA, USA). Glutathione (GSH) levels were determined using a GSH quantification assay kit (GSSG/GSH Quantification Kit; Dojindo, Tokyo, Japan). Biochemical measurements were carried out at room temperature using a spectrophotometer (Molecular Devices, Tokyo, Japan).

Study design

Liver cirrhosis model of rat fed WHP with DMN: Chronic phase

The control group (control diet with DMN treatment; n = 10) and the CN group (control diet without DMN as negative control for DMN; n = 3) received the control enteral diet, and the WHP group (WHP diet with DMN; n = 10) and WHPN group (WHP diet without DMN as negative control for DMN; n = 3)

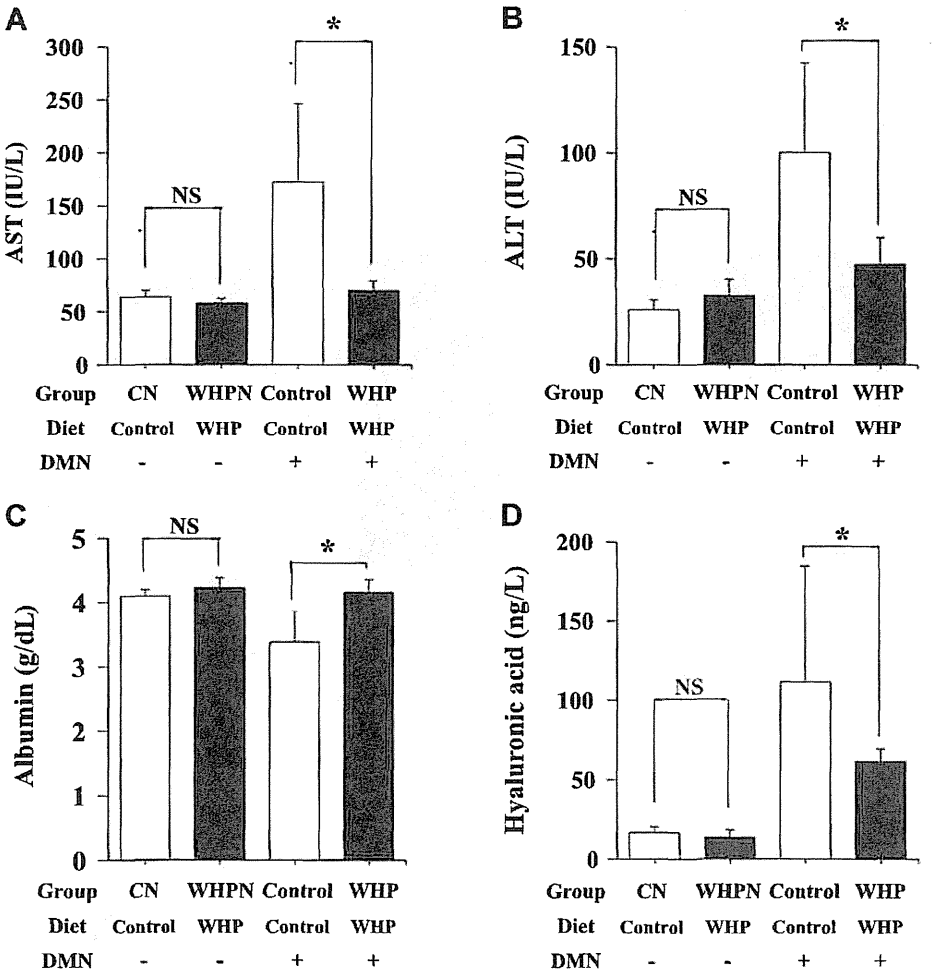

Fig. 4. Antifibrotic/cirrhotic effects of WHP in serum biochemical examinations (chronic phase). Increased serum levels of liver enzymes (A, B) and hyaluronic acid (D) were markedly attenuated, and albumin (C) was significantly higher in the WHP group than in the control group. *$P < 0.05$; NS, not significant ($P \geq 0.05$). CN, control diet without DMN as negative control for DMN; DMN, dimethylnitrosamine; WHP, whey-hydrolyzed peptide; WHPN, whey-hydrolyzed peptide diet without DMN as negative control for DMN.

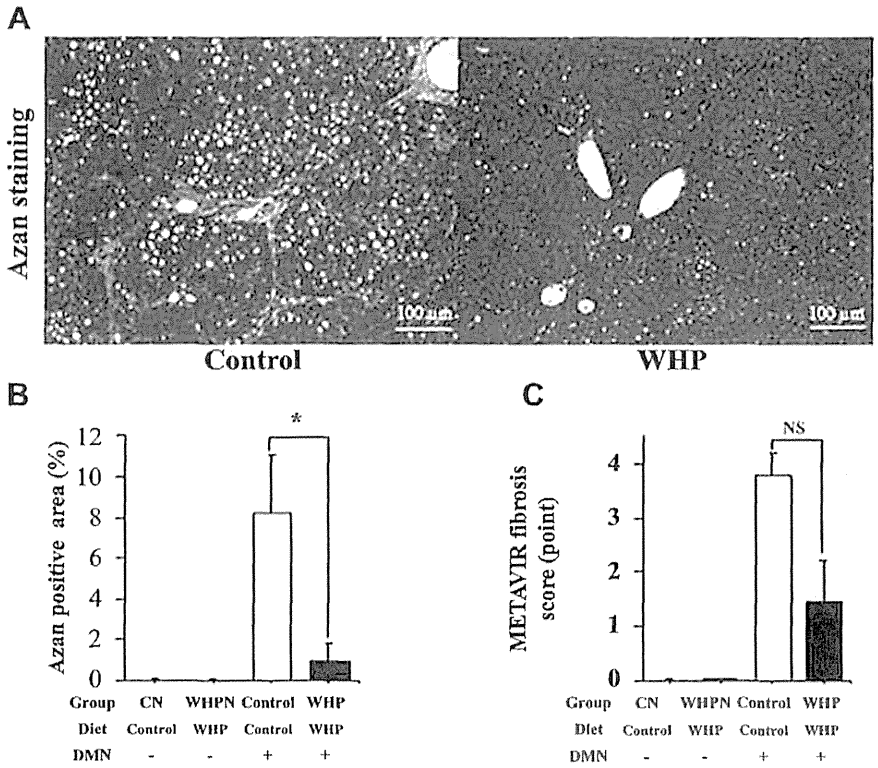

Fig. 5. Antifibrotic/cirrhotic effects of WHP in Azan staining (A, B) and Metavir fibrosis scores (C) (chronic phase). Azan-positive areas (A) and Metavir fibrosis scores (B) were significantly lower in the WHP group than in the control group. *$P < 0.05$. CN, control diet without DMN as negative control for DMN; DMN, dimethylnitrosamine; WHP, whey-hydrolyzed peptide; WHPN, whey-hydrolyzed peptide diet without DMN as negative control for DMN.

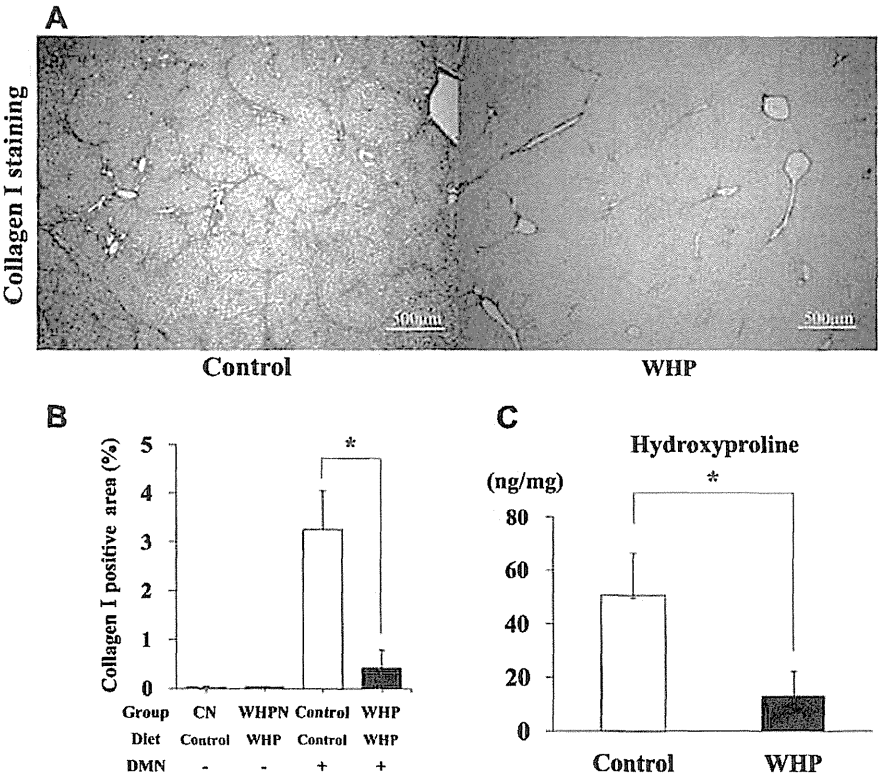

Fig. 6. Reduced rates of collagen expression in collagen I staining and hydroxyproline content in liver tissue by WHP treatment. Collagen I positive area (A, B) and hydroxyproline content in liver tissue (C) were significantly fewer in the WHP group than in the control group. *$P < 0.05$. CN, control diet without DMN as negative control for DMN; DMN, dimethylnitrosamine; WHP, whey-hydrolyzed peptide; WHPN, whey-hydrolyzed peptide diet without DMN as negative control for DMN.

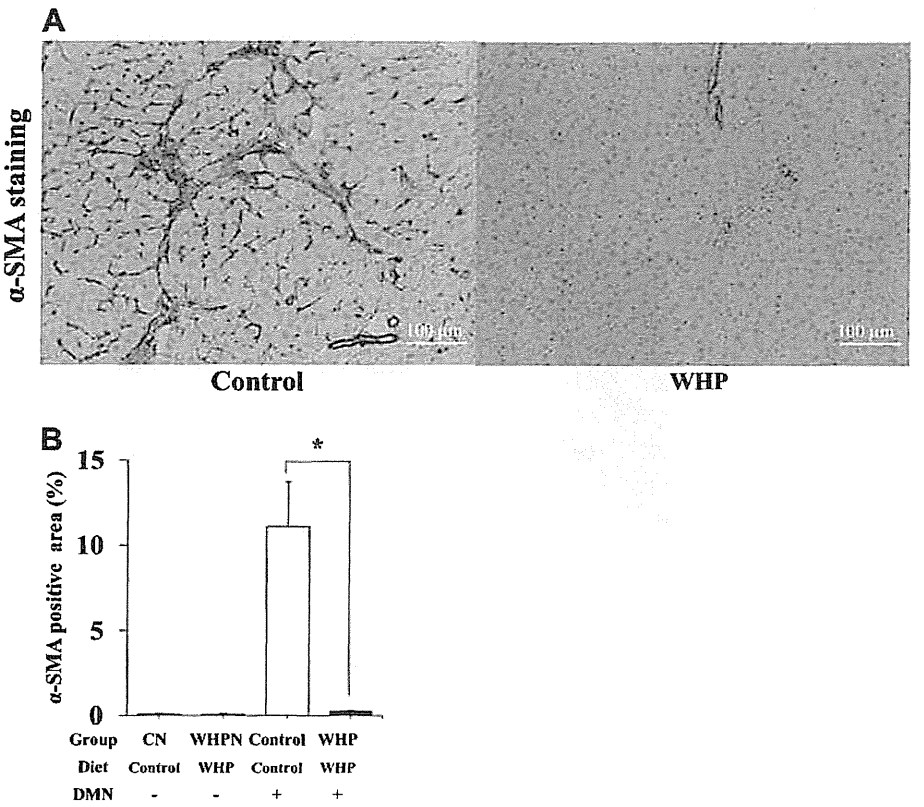

Fig. 7. Prevention of activation of hepatic stellate cells in α-SMA staining by WHP. The number of α-SMA-positive areas, which reflected to activated hepatic stellate cells, were significantly fewer in the WHP group than in the control group (A, B). *$P < 0.05$. DMN, dimethylnitrosamine; SMA, smooth muscle actin; WHP, whey-hydrolyzed peptide; WHPN, whey-hydrolyzed peptide diet without DMN as negative control for DMN.

received the WHP-enriched IMD ad libitum. Twelve d after the last DMN treatment, rats were sacrificed under isoflurane anesthesia (Escain; Mylan, Tokyo, Japan) (Fig. 1). At sacrifice, blood samples were collected from the abdominal aorta for conventional liver function tests (aspartate aminotransferase [AST], alanine aminotransferase [ALT], and total bilirubin [T-Bil]). Livers and spleens were excised and weighed for histopathology and immunochemistry.

To confirm the anti-inflammatory effect of WHP as previously reported, serum levels of IL-6, TNF-α, IL-10, IFN-γ and TGF-β, and also mRNA levels of IL-6 and TNF-α in liver tissue were measured. CYP2 E1 mRNA expression was measured to examine whether CYP2 E1 or a metabolic enzyme of DMN was regulated by WHP treatment. Also, MDA and GSH in liver tissue were measured to clarify whether WHP treatment was related to ROS reduction.

Liver cirrhosis model of rat fed WHP with DMN: Acute phase

The acute phase was also investigated before reaching the chronic phase. The control group (n = 6) received a control enteral diet, and the WHP group (n = 6) received a WHP-enriched IMD ad libitum. One d after the last DMN injection for 1 wk, rats were sacrificed (Fig. 1). At sacrifice, blood samples and liver tissues were collected. Serum levels of inflammatory cytokines were examined as described previously. For liver tissue, expression of mRNA of inflammatory cytokines and CYP2 E1, MDA, and GSH also were measured as described previously.

We performed additional experiments to evaluate the synergistic effects of TNF-α inhibitor (pentoxyfilline) in acute phase (pentoxifylline [PTX]-combined model). Rats were given DMN intraperitoneally and PTX [26–28] concomitantly for 3 consecutive days and sacrificed 24 h after last treatment in four experimental groups (n = 6 for each group, all groups were treated with DMN): control diet without PTX (ACDN), control diet with PTX (ACDP), WHP diet without PTX (AWDN), and WHP diet with PTX (AWDP). Serum conventional liver function tests, serum cytokines and histopathologic data were measured.

Hepatocyte-protective effect in vivo for isolated hepatocytes from rats fed WHP diet

Before hepatocyte isolation, rats were fed a control enteral diet (control diet group) or a WHP-enriched IMD (WHP diet group) for 1 wk. Hepatocytes were isolated from rat livers by a perfusion solution containing collagenase. Isolated hepatocytes were cultured on six-well plates. Medium was replaced 3 h after plating. Twelve hours later, 100 μmol/L of DMN was added [23], and cells were incubated. Three hours after DMN challenge, cultured hepatocytes were stained with Hoechst 33342 and propidium iodide. The propidium iodide-positive ratio was calculated to evaluate the degree of hepatocyte necrosis (Fig. 2A) [24].

Hepatocyte-protective effect in vitro for hepatocytes with WHP-added medium

Hepatocytes from rats fed commercial chow for 1 wk were isolated and cultured as above. Three hours after plating, medium was replaced with serum-free Medium 199 Earle's liquid without or with 500 μg/mL of casein peptide hydrolyzed by trypsin (CHP; Meiji Dairies Co.) or with 500 μg/mL of WHP (WHP by trypsin; Meiji Dairies Co.). Twelve hours later, 100 μM DMN or medium alone was added, and cells were incubated. Six experimental groups were defined as follows: Medium alone without peptide (D–P– group; n = 6), CHP alone (D–C+ group; n = 6), WHP alone (D–W+ group; n = 6), DMN alone (D+P– group; n = 6), DMN with CHP (D+C+ group; n = 6), and DMN with WHP (D+W+ group; n = 6). Three hours after DMN challenge, cultured hepatocytes were stained with Hoechst 33342 and propidium iodide. The propidium iodide-positive ratio was calculated as previously described (Fig. 2B).

Statistical analyses

Continuous values are expressed as means ± SD, and shown as the control group first and then the treated group. Data were statistically analyzed using Prism 5.0.1 (SAS Institute, Cary, NC, USA). Discrete variables were compared using a χ^2 test. Continuous variables were analyzed using a